

Accelerated Article Preview**Anti-SARS-CoV-2 receptor binding domain antibody evolution after mRNA vaccination**

Received: 25 July 2021

Accepted: 24 September 2021

Accelerated Article Preview Published
online 7 October 2021

Cite this article as: Cho, A. et al.

Anti-SARS-CoV-2 receptor binding domain
antibody evolution after mRNA vaccination.
Nature <https://doi.org/10.1038/s41586-021-04060-7> (2021).

Alice Cho, Frauke Muecksch, Dennis Schaefer-Babajew, Zijun Wang, Shlomo Finkin, Christian Gaebler, Victor Ramos, Melissa Cipolla, Pilar Mendoza, Marianna Agudelo, Eva Bednarski, Justin DaSilva, Irina Shimeliovich, Juan Dizon, Mridushi Daga, Katrina Millard, Martina Turroja, Fabian Schmidt, Fengwen Zhang, Tarek Ben Tanfous, Mila Jankovic, Thiago Y. Oliveria, Anna Gazumyan, Marina Caskey, Paul D. Bieniasz, Theodora Hatziioannou & Michel C. Nussenzweig

This is a PDF file of a peer-reviewed paper that has been accepted for publication. Although unedited, the content has been subjected to preliminary formatting. Nature is providing this early version of the typeset paper as a service to our authors and readers. The text and figures will undergo copyediting and a proof review before the paper is published in its final form. Please note that during the production process errors may be discovered which could affect the content, and all legal disclaimers apply.

Anti-SARS-CoV-2 receptor binding domain antibody evolution after mRNA vaccination

<https://doi.org/10.1038/s41586-021-04060-7>

Received: 25 July 2021

Accepted: 24 September 2021

Published online: 7 October 2021

Alice Cho^{1,4}, Frauke Muecksch^{2,4}, Dennis Schaefer-Babajew^{1,4}, Zijun Wang^{1,4}, Shlomo Fink^{1,4}, Christian Gaebler¹, Victor Ramos¹, Melissa Cipolla¹, Pilar Mendoza¹, Marianna Agudelo¹, Eva Bednarski², Justin DaSilva², Irina Shimeliovich¹, Juan Dizon¹, Mridushi Daga¹, Katrina Millard¹, Martina Turroja¹, Fabian Schmidt², Fengwen Zhang², Tarek Ben Tanfous¹, Mila Jankovic¹, Thiago Y. Oliveria¹, Anna Gazumyan¹, Marina Caskey^{1,3}, Paul D. Bieniasz^{2,3}, Theodora Hatzioannou^{2,3} & Michel C. Nussenzweig^{1,3}

Severe acute respiratory syndrome coronavirus 2 (SARS-CoV-2) infection produces B cell responses that continue to evolve for at least one year. During that time, memory B cells express increasingly broad and potent antibodies that are resistant to mutations found in variants of concern¹. As a result, vaccination of coronavirus disease 2019 (COVID-19) convalescent individuals with currently available mRNA vaccines produces high levels of plasma neutralizing activity against all variants tested^{1,2}. Here we examine memory B cell evolution 5 months after vaccination with either Moderna (mRNA-1273) or Pfizer-BioNTech (BNT162b2) mRNA vaccines in a cohort of SARS-CoV-2 naive individuals. Between prime and boost, memory B cells produce antibodies that evolve increased neutralizing activity, but there is no further increase in potency or breadth thereafter. Instead, memory B cells that emerge 5 months after vaccination of naive individuals express antibodies that are similar to those that dominate the initial response. While individual memory antibodies selected over time by natural infection have greater potency and breadth than antibodies elicited by vaccination, the overall neutralizing potency of plasma is greater following vaccination. These results suggest that boosting vaccinated individuals with currently available mRNA vaccines will increase plasma neutralizing activity but may not produce antibodies with equivalent breadth to those obtained by vaccinating convalescent individuals.

Between January 21 and July 20, 2021, we recruited 32 volunteers with no history of prior SARS-CoV-2 infection receiving either Moderna (mRNA-1273; n=8) or Pfizer-BioNTech (BNT162b2; n=24) mRNA vaccines for sequential blood donation. Matched samples were obtained at 2 or 3 time points. Individuals indicated as “prime” were sampled an average of 2.5 weeks after receiving their first vaccine dose. Individuals who completed their vaccination regimen were sampled after an average of 1.3 months after the boost (median=35.5 days) which is not statistically different from the 1.3 month sampling in our naturally infected cohort³ (median=38.5 days, p=0.21). Individuals sampled at 1.3 months were sampled again approximately 5 months after the second vaccine dose. The volunteers ranged in age from 23-78 years (median=34.5 years), 53% were male and 47% female (for details see Methods and Supplementary Tables 1 and 2).

Plasma binding and neutralization assays

Plasma IgM, IgG, and IgA responses to SARS-CoV-2 receptor binding domain (RBD) were measured by enzyme linked immunosorbent assay

(ELISA)³. As reported by others^{2,4-6} there was a significant increase in IgG reactivity to RBD between prime and boost (p<0.0001, Fig. 1a). IgM and IgA titers were lower than IgG titers and remained low after the second vaccine dose (Extended Data Fig. 1a, b). The magnitude of the response was inversely correlated with age after the prime (r=-0.54, p=0.005), but in this limited sample set the age difference was no longer significant at 1.3 or 5 months after the second vaccine dose (Extended Data Fig. 1c, d). Between 1.3 and 5 months after the boost, anti-RBD titers of IgG and IgA decreased significantly. IgG titers decreased by an average of 4.3-fold (range: 1.7- to 10.2-fold) and the loss of activity was directly correlated to the time after vaccination (p<0.0001, Fig. 1a, Extended Data Fig. 1a, b, e).

Neutralizing activity was measured using HIV-1 pseudotyped with the SARS-CoV-2 spike^{1,3,7,8}. Naïve individuals showed variable responses to the initial vaccine dose with a geometric mean half-maximal neutralizing titer (NT₅₀) of 171 (Fig. 1b, Supplementary Table 2). The magnitude of the neutralizing responses to the initial vaccine dose in naïve volunteers was inversely correlated with age (r=-0.39, p=0.05, Fig. 1c). Both binding and neutralizing responses to the second vaccine dose were

¹Laboratory of Molecular Immunology, The Rockefeller University, New York, NY, USA. ²Laboratory of Retrovirology, The Rockefeller University, New York, NY, USA. ³Howard Hughes Medical Institute, New York, NY, USA. ⁴These authors contributed equally: Alice Cho, Frauke Muecksch, Dennis Schaefer-Babajew, Zijun Wang and Shlomo Fink. ✉e-mail: mcaskey@rockefeller.edu; pbieniasz@rockefeller.edu; thatziio@rockefeller.edu; nussen@rockefeller.edu

correlated to the prime ($r=0.46$, $p=0.02$, Extended Data Fig. 1f; $r=0.54$, $p=0.003$, Extended Data Fig. 1g) and produced a nearly 12-fold increase in the geometric mean neutralizing response that was similar in males and females and eliminated the age-related difference in neutralizing activity in the individuals in this cohort (Fig. 1b, Extended Data Fig. 1h, Fig. 1c, Extended Data Fig. 1i). 1.3 and 5 months after the boost naïve vaccinees had 4.9- and 3.6 fold higher neutralizing titers than a cohort of infected individuals measured 1.3³- and 6.2⁷-months after symptom onset, respectively ($p<0.0001$, Fig. 1b). Neutralizing responses were directly correlated to IgG anti-RBD titers ($r=0.96$, $p<0.0001$, Extended Data Fig. 1j). Thus, the data obtained from this cohort agree with prior observations showing a significant increase in plasma neutralizing activity that are correlated with improved vaccine efficacy in naïve individuals that receive the second dose of mRNA vaccine^{2,6,9,10} and higher neutralizing titers in fully vaccinated than infected individuals^{2,6}.

The 28 individuals assayed 5 months after vaccination had a 7.1-fold decrease in geometric mean neutralizing titer from their 1.3-month measurement ($p<0.0001$, Fig. 1b), with a range of 1.4- to 27-fold. Neutralizing activity was inversely correlated with the time from vaccination ($r=-0.82$, $p<0.0001$, Fig. 1d), and directly correlated to IgG anti-RBD binding titers when assessed 5 months after vaccination (Extended Data Fig. 1k). As reported by others¹¹, the ratio of binding to neutralizing serum titers was significantly higher in vaccinated than convalescent individuals at the 1.3-month time point ($p<0.0001$, Extended Data Fig. 1l). However, the difference was no longer apparent at the later time point (Extended Data Fig. 1l).

We and others showed that the neutralizing responses elicited by mRNA vaccination are more potent against the original Wuhan Hu-1 strain than for some of the currently circulating variants of concern^{2,12-14}. To confirm these observations, we measured the neutralizing activity of 15 paired plasmas from naïve individuals 1.3 and 5 months after the second vaccine dose against B.1.1.7 (alpha variant), B.1.351 (beta variant), B.1.526 (iota variant), P.1 (gamma variant) and B.1.617.2 (delta variant). Consistent with previous reports^{13,15-17} the neutralizing activity against the variants was lower than against the original Wuhan Hu-1 strain (Fig. 1e, Supplementary Table 3). Initial geometric mean neutralizing titers at 1.3 months against B.1.351, B.1.1.7, B.1.526, P.1 and B.1.617.2 were 5.7, 1.8, 1.1, 1.4 and 2.7-fold lower than against Wuhan-Hu respectively (Fig. 1e). In the months following vaccination there was a decrease in neutralizing activity against Wuhan Hu-1 (R683G) and all the variants with geometric mean neutralizing titers for WT, B.1.351, B.1.1.7, B.1.526, P.1 and B.1.617.2 decreasing by 2.9-, 1.8-, 2.3-, 2.9-, 2.4- and 2.6-fold, respectively (Fig. 1e, Supplementary Table 3).

Monoclonal Antibodies

Circulating antibodies produced by plasma cells can prevent infection if present at sufficiently high concentrations at the time of exposure. In contrast, the memory B cell compartment contains long lived antigen-specific B cells that mediate rapid recall responses that contribute to long term protection¹⁸. To examine the nature of the memory compartment elicited by one or two mRNA vaccine doses and its evolution after 5 months we used flow cytometry to enumerate B cells expressing receptors that bind to Wuhan Hu-1 (wild type, WT) and the B.1.351 K417N/E484K/N501Y variant RBDs (Fig. 2a, b, Extended Data Fig. 2). Although neutralizing antibodies develop to other parts of the spike (S) protein we focused on RBD because it is the dominant target of the memory antibody neutralizing response^{19,20}. Wuhan-Hu RBD-specific memory B cells developed after the prime in all volunteers examined and their numbers increased for up to 5 months after vaccination (Fig. 2a). Memory B cells binding to the B.1.351 K417N/E484K/N501Y variant RBD were detectable but in lower numbers than wild type RBD-binding B cells in all samples examined (Fig. 2b). Whereas IgG memory cells increased after the boost, IgM-expressing memory B cells that made up 23% of the memory compartment after the prime were

nearly absent after boosting (Extended Data Fig. 3a). Finally, circulating RBD-specific plasmablasts were readily detected after the prime but were infrequent after the boost (Extended Data Fig. 2d, Extended Data Fig. 3b).

The memory compartment continues to evolve up to one year after natural infection with selective enrichment of cells producing broad and potent neutralizing antibodies¹. To determine how the memory compartment evolves after vaccination, we obtained 2327 paired antibody sequences from 11 individuals sampled at the time points described above (Fig. 2c, Extended Data Fig. 3c-e, Supplementary Table 4). As expected *IGHV3-30* and *IGHV3-53* were over-represented after the first and second vaccine dose and remained over-represented 5 months after vaccination²¹⁻²³ (Extended Data Fig. 4).

All individuals examined showed expanded clones of memory B cells that expressed closely related *IGHV* and *IGHL* genes (Fig. 2c, Extended Data Fig. 3c-e, Extended Data Fig. 4). Paired prime and 1.3 month post boost samples showed expanded clones of memory B cells some of which were shared across plasmablasts, IgM and IgG prime, and IgG boost memory cells (Extended Data Fig. 3c and 5). Thus, the cell fate decision controlling the germinal center versus plasmablast decision is not entirely affinity dependent since cells with the same initial affinity can enter both compartments to produce clonal relatives²⁴.

The relative fraction of memory cells found in expanded clones varied between prime and boost and between individuals and decreased over time (Fig. 2c, Extended Data Fig. 3d-f). Overall, clones represented 30%, 21%, and 9.7% of all sequences after prime, 1.3- and 5-month time points respectively (Extended Data Fig. 3f). Nevertheless, clones of memory B cells continued to evolve for up to 5 months in vaccinated individuals as evidenced by the appearance of unique clones. Notably, unique clones appearing after 1.3 and 5 months represent a greater or equal fraction of the total memory B cell pool than the persisting clones (Fig. 2c, Extended Data Fig. 3d, e, g, 16% vs 9.6% and 5.1% vs 4.7%, respectively). Finally, memory B cells emerging after the boost showed significantly higher levels of somatic mutations than plasmablasts or memory B cells isolated after the prime, and they continue to accumulate mutations up to 5 months post-boost (Fig. 2d, Extended Data Fig. 3h, i). In conclusion the memory B cell compartment continues to evolve for up to 5 months after mRNA vaccination.

Neutralizing Activity of Monoclonal Antibodies

We performed ELISAs to confirm that the antibodies isolated from memory B cells bind to RBD (Extended Data Fig. 6). 458 antibodies were tested by ELISA including: 88 isolated after the first vaccine dose; 210 isolated after the boost; and 160 isolated from individuals that had been fully vaccinated 5 months earlier. Among the 458 antibodies tested 430 (94%) bound to the Wuhan Hu-1 RBD indicating that the method used to isolate RBD-specific memory B cells was highly efficient (Supplementary Table 5-6). The geometric mean ELISA half-maximal concentration (EC_{50}) of the antibodies obtained after prime, and 1.3- and 5-months after the second dose was 3.5, 2.9 and 2.7 ng/ml respectively, suggesting no major change in binding over time after vaccination (Extended Data Fig. 6, Supplementary Table 5-6).

430 RBD-binding antibodies were tested for neutralizing activity using HIV-1 pseudotyped with the SARS-CoV-2 spike^{3,8}. The geometric mean half-maximal inhibitory concentration (IC_{50}) of the RBD-specific memory antibodies improved from 376 ng/ml to 153 ng/ml between the first and second vaccine dose ($p=0.0005$, Fig. 3a). The improvement was reflected in all clones (IC_{50} 377 vs. 171 ng/ml, $p=0.01$ Extended Data Fig. 7a), persisting clones (IC_{50} 311 vs. 168, Fig. 3b, Supplementary Table 6), unique clones (IC_{50} 418 vs. 165 ng/ml, $p=0.03$, Fig. 3c), and single antibodies (IC_{50} 374 vs. 136 ng/ml, Extended Data Fig. 7b). The increase in neutralizing activity between the first and second vaccine dose was associated with a decrease in the percentage of non-neutralizing antibodies (defined as $IC_{50} >1000$ ng/ml)

and increased representation of neutralizing antibodies ($p = 0.003$, Fig. 3a). In conclusion, memory B cells recruited after the second dose account for most of the improvement in neutralizing activity in this compartment between the 2 vaccine doses. Thus, in addition to the quantitative improvement in serum neutralizing activity there is also an improvement in the neutralizing activity of the antibodies expressed in the memory compartment after boosting.

In contrast, there was no significant improvement in neutralizing activity of the monoclonal antibodies obtained between 1.3 and 5 months after vaccination ($p > 0.99$, Fig. 3a). Although there was some improvement among B cell clones, which was accounted for by the small minority of persisting clones, neither was significant ($p = 0.58$ and 0.46 , Extended Data Fig. 7a, Fig. 3b, Supplementary table 6). In contrast, memory antibodies obtained from convalescent individuals showed improved neutralizing activity between 1.3³ and 6.2 months⁷ with IC_{50} of 171 ng/ml to 116 ng/ml (Fig. 3a), which improved further after 1 year¹. This improvement was due to increased neutralizing activity among persisting clones ($p = 0.003$, Fig. 3b).

Affinity, Epitopes and Neutralization Breadth

To examine affinity maturation after vaccination, we performed bi-layer interferometry (BLI) experiments using the Wuhan Hu-1 RBD³. 147 antibodies were assayed, 30 obtained after the prime, 74 1.3-months after boosting, and 43 5-months after the boost. Geometric mean IC_{50} s were comparable for the antibodies obtained from the 1.3- and 5-month time points (Extended Data Fig. 8a). Overall, there was a 3- and 7.5 fold increase in affinity between the antibodies obtained between the first 2, and second 2 time points respectively (Fig. 4a). After 5 months the affinity of the antibodies obtained from vaccinated individuals was similar to antibodies obtained from naturally infected volunteers (Fig 4a). However, there was no correlation between affinity and neutralizing activity of the antibodies tested at any of the 3 time points (Extended Data Fig. 8b).

We also compared the affinities of pairs of antibodies obtained from persisting clones between 1.3 and 5 months after vaccination. Persisting clones obtained at 1.3 and 5 months from vaccinated individuals showed a median 4.5-fold increase in affinity ($p < 0.0001$, Fig. 4b). In contrast, a comparable group of persisting clonal antibodies obtained from convalescent individuals 1.3 and 6.2 months after infection showed a median 11.2-fold increase in affinity ($p = 0.002$, Fig. 4b).

To determine whether the epitopes targeted by the monoclonal antibodies were changing over time, we performed BLI experiments in which a preformed antibody-RBD complex was exposed to a second monoclonal targeting one of 4 classes of structurally defined epitopes¹³ (see schematic in Extended Data Fig. 8c). There was no significant change in the distribution of targeted epitopes among 52 randomly selected antibodies with comparable neutralizing activity obtained from the 1.3- and 5-month time points (Extended Data Fig. 8d, e, Extended Data Fig. 9).

In addition to the increase in potency, the neutralizing breadth of memory antibodies obtained from persisting clones from convalescent individuals increases with time after infection^{1,7,25}. To determine whether there is a similar increase in breadth with time after vaccination, we selected 20 random antibodies from the prime or 1.3 months after boost, with representative levels of activity against the original Wuhan Hu-1 strain, and measured their neutralization potency against a panel of pseudotypes encoding RBD mutations which were selected for resistance to different RBD antibody classes and/or are associated with circulating variants of concern (Extended Data Table 1). There was little change in breadth between prime and 1.3 months after boost, with only a small increase in resistance to K417N and A475V substitutions (Extended Data Table 1, Supplementary Table 7).

In addition, we assayed 19 pairs of neutralizing antibodies expressed by persisting clones obtained 1.3 and 5 months after vaccination against

the same mutant pseudotype viruses (Fig. 4c, Supplementary Table 8). They were compared to 7 previously reported²⁵, plus 9 additional pairs of antibodies obtained from convalescent individuals at 1.3- and 6.2-month time points (Fig. 4d, Supplementary Table 8). Whereas only 36 of 190 (19%) of the vaccinee antibody-mutant combinations showed improved potency, 95 of the 160 (59%) convalescent pairs did so ($p < 0.0001$, Fig. 4c–e). Moreover, only 4 of the 19 (21%) vaccine antibody pairs showed improved potency against pseudotypes carrying B.1.617.2 (delta variant)-specific RBD amino acid substitutions (L452R/T478K), while 11 out of 16 (69%) of the convalescent antibody pairs showed improved activity against this virus ($p = 0.007$, Fig. 4c–e). We conclude that there is less increase in breadth in the months after mRNA vaccination than in a similar interval in naturally infected individuals.

Circulating antibodies are produced by an initial burst of short-lived plasmablasts^{26,27}, and maintained by plasma cells with variable longevity^{28,29}. SARS-CoV-2 infection or mRNA vaccination produces an early peak antibody response that decreases by 5-10-fold after 5 months^{7,30–34}. Notably, neutralization titres elicited by vaccination exceed those of COVID-19 recovered individuals at all comparable time points assayed. Nevertheless, neutralizing potency against variants is significantly lower than against Wuhan Hu-1, with up to 5-10-fold reduced activity against the B.1.351 variant^{5,6,13,14,35}. Taken together with the overall decay in neutralizing activity there can be 1-2 orders of magnitude decrease in serum neutralizing activity after 5 or 6 months against variants when compared to the peak of neutralizing activity against Wuhan Hu-1. Thus, antibody mediated protection against variants is expected to wane significantly over a period of months, consistent with reports of reinfection in convalescent individuals and breakthrough infection by variants in fully vaccinated individuals^{36–39}.

In contrast to circulating antibodies, memory B cells are responsible for rapid recall responses^{40–42}, and the number of cells in this compartment is relatively stable over the first 5-6 months after mRNA vaccination or natural infection^{7,43}. In both cases memory B cells continue to evolve as evidenced by increasing levels of somatic mutation and emergence of unique clones.

The memory response would be expected to protect individuals that suffer breakthrough infection from developing serious disease. Both natural infection and mRNA vaccination produce memory antibodies that evolve increased affinity. However, vaccine-elicited memory monoclonal antibodies show more modest neutralizing potency and breadth than those that developed after natural infection¹⁷. Notably, the difference between the memory compartment that develops in response to natural infection vs mRNA vaccination reported above is consistent with the higher level of protection from variants conferred by natural infection³⁹.

There are innumerable differences between natural infection and mRNA vaccination that could account for the differences in antibody evolution over time. These include but are not limited to: 1. Route of antigen delivery, respiratory tract vs. intra-muscular injection^{44,45}; 2. The physical nature of the antigen, intact virus vs. conformationally stabilized prefusion S protein⁴⁶; 3. Antigen persistence, weeks in the case of natural infection⁷ vs. hours to days for mRNA⁴⁷. Each of these could impact on B cell evolution and selection directly, and indirectly through differential T cell recruitment.

The increase in potency and breadth in the memory compartment that develops after natural infection accounts for the exceptional responses to Wuhan Hu-1 and its variants that convalescent individuals develop when boosted with mRNA vaccines^{1,5}. The expanded memory B cell compartment in mRNA vaccinees should also produce high titers of neutralizing antibodies when vaccinees are boosted or when they are re-exposed to the virus⁴⁸. Boosting vaccinated individuals with currently available mRNA vaccines should produce strong responses that mirror or exceed their initial vaccine responses to Wuhan-Hu but with similarly decreased coverage against variants. Whether an additional boost with Wuhan-Hu-based or variant vaccines or re-infection will also

elicit development of memory B cells expressing antibodies showing increased breadth remains to be determined. Finally, timing an additional boost for optimal responses depends on whether the objective is to prevent infection or disease⁴⁹. Given the current rapid emergence of SARS-CoV-2 variants, boosting to prevent infection would likely be needed on a time scale of months. The optimal timing for boosting to prevent serious disease will depend on the stability and further evolution of the memory B cell compartment.

Online content

Any methods, additional references, Nature Research reporting summaries, source data, extended data, supplementary information, acknowledgements, peer review information; details of author contributions and competing interests; and statements of data and code availability are available at <https://doi.org/10.1038/s41586-021-04060-7>.

- Wang, Z. et al. Naturally enhanced neutralizing breadth against SARS-CoV-2 one year after infection. *Nature*, <https://doi.org/10.1038/s41586-021-03696-9> (2021).
- Goel, R. R. et al. Distinct antibody and memory B cell responses in SARS-CoV-2 naive and recovered individuals following mRNA vaccination. *Sci Immunol* **6**, <https://doi.org/10.1126/sciimmunol.abi6950> (2021).
- Robbiani, D. F. et al. Convergent antibody responses to SARS-CoV-2 in convalescent individuals. *Nature* **584**, 437–442, <https://doi.org/10.1038/s41586-020-2456-9> (2020).
- Apostolidis, S. A. et al. Altered cellular and humoral immune responses following SARS-CoV-2 mRNA vaccination in patients with multiple sclerosis on anti-CD20 therapy. *medRxiv*, 2021.2006.2023.21259389, <https://doi.org/10.1101/2021.06.23.21259389> (2021).
- Sokal, A. et al. Memory B cells control SARS-CoV-2 variants upon mRNA vaccination of naive and COVID-19 recovered individuals. *bioRxiv*, 2021.2006.2017.448459, <https://doi.org/10.1101/2021.06.17.448459> (2021).
- Turner, J. S. et al. SARS-CoV-2 mRNA vaccines induce persistent human germinal centre responses. *Nature*, <https://doi.org/10.1038/s41586-021-03738-2> (2021).
- Gaebler, C. et al. Evolution of antibody immunity to SARS-CoV-2. *Nature* **591**, 639–644, <https://doi.org/10.1038/s41586-021-03207-w> (2021).
- Schmidt, F. et al. Measuring SARS-CoV-2 neutralizing antibody activity using pseudotyped and chimeric viruses. *J Exp Med* **217**, <https://doi.org/10.1084/jem.20201181> (2020).
- Pilishvili, T. et al. Interim Estimates of Vaccine Effectiveness of Pfizer-BioNTech and Moderna COVID-19 Vaccines Among Health Care Personnel - 33 U.S. Sites, January-March 2021. *MMWR Morb Mortal Wkly Rep* **70**, 753–758, <https://doi.org/10.15585/mmwr.mm7020e2> (2021).
- Lopez Bernal, J. et al. Effectiveness of Covid-19 Vaccines against the B.1.617.2 (Delta) Variant. *N Engl J Med*, <https://doi.org/10.1056/NEJMoa2108891> (2021).
- Amanat, F. et al. SARS-CoV-2 mRNA vaccination induces functionally diverse antibodies to NTD, RBD, and S2. *Cell* **184**, 3936–3948 e3910, <https://doi.org/10.1016/j.cell.2021.06.005> (2021).
- Reynolds, C. J. et al. Prior SARS-CoV-2 infection rescues B and T cell responses to variants after first vaccine dose. *Science*, <https://doi.org/10.1126/science.abh1282> (2021).
- Wang, Z. et al. mRNA vaccine-elicited antibodies to SARS-CoV-2 and circulating variants. *Nature* **592**, 616–622, <https://doi.org/10.1038/s41586-021-03324-6> (2021).
- Stamatatos, L. et al. mRNA vaccination boosts cross-variant neutralizing antibodies elicited by SARS-CoV-2 infection. *Science*, <https://doi.org/10.1126/science.abg9175> (2021).
- West, A. P. et al. Detection and characterization of the SARS-CoV-2 lineage B.1.526 in New York. *bioRxiv*, <https://doi.org/10.1101/2021.02.14.431043> (2021).
- Edara, V. V. et al. Infection and Vaccine-Induced Neutralizing-Antibody Responses to the SARS-CoV-2 B.1.617 Variants. *N Engl J Med*, <https://doi.org/10.1056/NEJMoa2107799> (2021).
- Planas, D. et al. Reduced sensitivity of SARS-CoV-2 variant Delta to antibody neutralization. *Nature*, <https://doi.org/10.1038/s41586-021-03777-9> (2021).
- Victoria, G. D. & Nussenzweig, M. C. Germinal centers. *Annu Rev Immunol* **30**, 429–457, <https://doi.org/10.1146/annurev-immunol-020711-075032> (2012).
- Dugan, H. L. et al. Profiling B cell immunodominance after SARS-CoV-2 infection reveals antibody evolution to non-neutralizing viral targets. *Immunity* **54**, 1290–1303 e1297, <https://doi.org/10.1016/j.immuni.2021.05.001> (2021).
- Li, D. et al. In vitro and in vivo functions of SARS-CoV-2 infection-enhancing and neutralizing antibodies. *Cell* **184**, 4203–4219 e4232, <https://doi.org/10.1016/j.cell.2021.06.021> (2021).
- Brouwer, P. J. M. et al. Potent neutralizing antibodies from COVID-19 patients define multiple targets of vulnerability. *Science* **369**, 643–650, <https://doi.org/10.1126/science.abc5902> (2020).
- Kreer, C. et al. Longitudinal Isolation of Potent Near-Germline SARS-CoV-2-Neutralizing Antibodies from COVID-19 Patients. *Cell* **182**, 843–854 e812, <https://doi.org/10.1016/j.cell.2020.06.044> (2020).
- Seydoux, E. et al. Analysis of a SARS-CoV-2-Infected Individual Reveals Development of Potent Neutralizing Antibodies with Limited Somatic Mutation. *Immunity* **53**, 98–105 e105, <https://doi.org/10.1016/j.immuni.2020.06.001> (2020).
- Taylor, J. J., Pape, K. A., Steach, H. R. & Jenkins, M. K. Humoral immunity. Apoptosis and antigen affinity limit effector cell differentiation of a single naive B cell. *Science* **347**, 784–787, <https://doi.org/10.1126/science.aaa1342> (2015).
- Muecksch, F. et al. Affinity maturation of SARS-CoV-2 neutralizing antibodies confers potency, breadth, and resilience to viral escape mutations. *Immunity* **54**, 1853–1868 e1857, <https://doi.org/10.1016/j.immuni.2021.07.008> (2021).
- Li, G. M. et al. Pandemic H1N1 influenza vaccine induces a recall response in humans that favors broadly cross-reactive memory B cells. *Proc Natl Acad Sci U S A* **109**, 9047–9052, <https://doi.org/10.1073/pnas.1118979109> (2012).
- Wrarmert, J. et al. Rapid cloning of high-affinity human monoclonal antibodies against influenza virus. *Nature* **453**, 667–671, <https://doi.org/10.1038/nature06890> (2008).
- Amanna, I. J., Carlson, N. E. & Slifka, M. K. Duration of humoral immunity to common viral and vaccine antigens. *N. Engl. J. Med.* **357**, 1903–1915, <https://doi.org/10.1056/NEJMoa066092> (2007).
- Halliley, J. L. et al. Long-Lived Plasma Cells Are Contained within the CD19⁺-JCD38(hi) CD138⁺ Subset in Human Bone Marrow. *Immunity* **43**, 132–145, <https://doi.org/10.1016/j.immuni.2015.06.01> (2015).
- Dan, J. M. et al. Immunological memory to SARS-CoV-2 assessed for up to 8 months after infection. *Science* **371**, <https://doi.org/10.1126/science.abf4063> (2021).
- Sakharkar, M. et al. Prolonged evolution of the human B cell response to SARS-CoV-2 infection. *Sci Immunol* **6**, <https://doi.org/10.1126/sciimmunol.abg6916> (2021).
- Widge, A. T. et al. Durability of Responses after SARS-CoV-2 mRNA-1273 Vaccination. *N. Engl. J. Med.* **384**, 80–82, <https://doi.org/10.1056/NEJMoa2032195> (2021).
- Wajnberg, A. et al. Robust neutralizing antibodies to SARS-CoV-2 infection persist for months. *Science* **370**, 1227–1230, <https://doi.org/10.1126/science.abd7728> (2020).
- Pegu, A. et al. Durability of mRNA-1273-induced antibodies against SARS-CoV-2 variants. *bioRxiv*, <https://doi.org/10.1101/2021.05.13.444010> (2021).
- Chen, R. E. et al. Resistance of SARS-CoV-2 variants to neutralization by monoclonal and serum-derived polyclonal antibodies. *Nat. Med.* **27**, 717–726, <https://doi.org/10.1038/s41591-021-01294-w> (2021).
- Abu-Raddad, L. J., Chemaitelly, H., Butt, A. A. & National Study Group for, C.-V. Effectiveness of the BNT162b2 Covid-19 Vaccine against the B.1.1.7 and B.1.351 Variants. *N. Engl. J. Med.* **385**, 187–189, <https://doi.org/10.1056/NEJMoa2104974> (2021).
- Hacisuleyman, E. et al. Vaccine Breakthrough Infections with SARS-CoV-2 Variants. *N. Engl. J. Med.* **384**, 2212–2218, <https://doi.org/10.1056/NEJMoa2105000> (2021).
- Lumley, S. F. et al. Antibody Status and Incidence of SARS-CoV-2 Infection in Health Care Workers. *N. Engl. J. Med.* **384**, 533–540, <https://doi.org/10.1056/NEJMoa2034545> (2021).
- Gazit, S. et al. Comparing SARS-CoV-2 natural immunity to vaccine-induced immunity: reinfections versus breakthrough infections. *medRxiv*, 2021.2008.2024.21262415, <https://doi.org/10.1101/2021.08.24.21262415> (2021).
- Mesin, L. et al. Restricted Clonality and Limited Germinal Center Reentry Characterize Memory B Cell Reactivation by Boosting. *Cell* **180**, 92–106 e111, <https://doi.org/10.1016/j.cell.2019.11.032> (2020).
- Pape, K. A., Taylor, J. J., Maul, R. W., Gearhart, P. J. & Jenkins, M. K. Different B cell populations mediate early and late memory during an endogenous immune response. *Science* **331**, 1203–1207, <https://doi.org/10.1126/science.1201730> (2011).
- Viant, C. et al. Antibody Affinity Shapes the Choice between Memory and Germinal Center B Cell Fates. *Cell* **183**, 1298–1311 e1211, <https://doi.org/10.1016/j.cell.2020.09.063> (2020).
- Sokal, A. et al. Maturation and persistence of the anti-SARS-CoV-2 memory B cell response. *Cell* **184**, 1201–1213 e1214, <https://doi.org/10.1016/j.cell.2021.01.050> (2021).
- Feng, L. et al. An adenovirus-vectored COVID-19 vaccine confers protection from SARS-CoV-2 challenge in rhesus macaques. *Nat. Commun.* **11**, 4207, <https://doi.org/10.1038/s41467-020-18077-5> (2020).
- Hassan, A. O. et al. A Single-Dose Intranasal ChAd Vaccine Protects Upper and Lower Respiratory Tracts against SARS-CoV-2. *Cell* **183**, 169–184 e113, <https://doi.org/10.1016/j.cell.2020.08.026> (2020).
- Greaney, A. J. et al. Antibodies elicited by mRNA-1273 vaccination bind more broadly to the receptor binding domain than do those from SARS-CoV-2 infection. *Sci Transl Med* **13**, <https://doi.org/10.1126/scitranslmed.abi9915> (2021).
- Pardi, N. et al. Expression kinetics of nucleoside-modified mRNA delivered in lipid nanoparticles to mice by various routes. *J. Control. Release* **217**, 345–351, <https://doi.org/10.1016/j.jconrel.2015.08.007> (2015).
- Wu, K. et al. Preliminary Analysis of Safety and Immunogenicity of a SARS-CoV-2 Variant Vaccine Booster. *medRxiv*, 2021.2005.2005.21256716, <https://doi.org/10.1101/2021.05.05.21256716> (2021).
- Khoury, D. S. et al. Neutralizing antibody levels are highly predictive of immune protection from symptomatic SARS-CoV-2 infection. *Nat. Med.* **27**, 1205–1211, <https://doi.org/10.1038/s41591-021-01377-8> (2021).
- Wu, F. et al. A new coronavirus associated with human respiratory disease in China. *Nature* **579**, 265–269, <https://doi.org/10.1038/s41586-020-2008-3> (2020).

Publisher's note Springer Nature remains neutral with regard to jurisdictional claims in published maps and institutional affiliations.

© The Author(s), under exclusive licence to Springer Nature Limited 2021

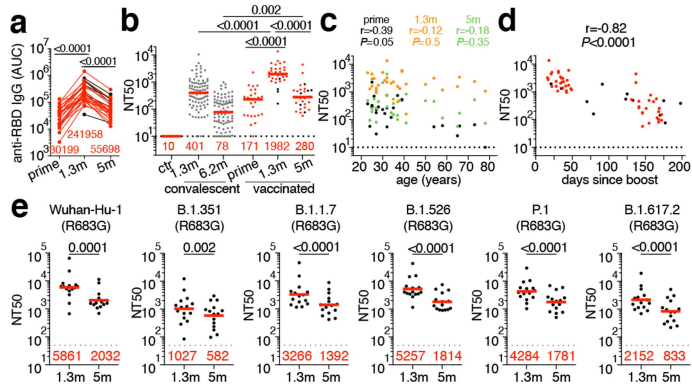


Fig. 1 | Plasma ELISAs and neutralizing activity. a, Graph shows area under the curve (AUC) for plasma IgG antibody binding to SARS-CoV-2 RBD after prime, and 1.3 months (m) and 5 months (m) post-second vaccination for n=32 paired samples. Samples without a prime value are shown in black. **b**, NT50 values in plasma from pre-pandemic controls (ctr, n=3), convalescent individuals 1.3m³ and 6.2m⁷ after infection (grey), and vaccinated individuals (n=32) after prime, and 1.3- and 5-months after receiving 2 doses of mRNA vaccination. Samples without a prime value are shown in black. **c**, NT50 values (Y-axis) vs. age (years, X-axis) in n=32 individuals after prime (black), or 1.3 months (1.3m, orange) or 5 months (5m, green) after boosting with an mRNA vaccine. **d**, Graph shows NT50 values (Y-axis) vs. days after boost (X-axis) in n=32 individuals receiving two doses of an mRNA vaccine. Samples without a prime value are shown in black. **e**, Plasma neutralizing activity against indicated SARS-CoV-2 variants of interest/concern (n=15 paired samples at 1.3- and 5-months after full vaccination). Refer to Methods for a list of all substitutions/deletions/insertions in the spike variants. All experiments were performed at least in duplicate. Red bars and values in **a**, **b**, and **e** represent geometric mean values. Statistical significance in **a**, **b**, and **e** was determined by two-tailed Kruskal-Wallis test with subsequent Dunn's multiple comparisons, and in **c** and **d** by two-tailed Spearman correlation test.

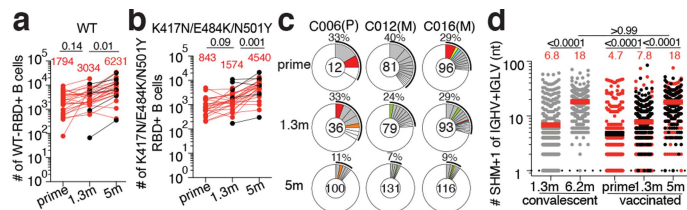


Fig. 2 | Anti-SARS-CoV-2 RBD B cells after vaccination. a, b, Graphs summarizing **a**, the number of Wuhan-Hu RBD (WT)-specific memory B cells or **b**, the number of antigen-specific memory B cells cross-reactive with both WT and K417N/E484K/N501Y RBD mutant per 10 million B cells for $n=32$ individuals after prime, 1.3- and 5-months after full vaccination. Samples without a prime value are shown in black. **c**, Pie charts show the distribution of IgG antibody sequences obtained from memory B cells from 3 representative individuals after prime and 1.3-months or 5-months post-boost. Additional pie charts can be found in Extended Data Fig. 3. The number inside the circle indicates the number of sequences analyzed for the individual denoted above the circle, with Pfizer vaccinees indicated by (P) and Moderna by (M). Pie slice size is proportional to the number of clonally related sequences. The black outline and associated numbers indicate the percentage of clonally expanded sequences detected at each time point. Colored slices indicate persisting clones (same *IGHV* and *IGLV* genes, with highly similar CDR3s) found at more than one timepoint within the same individual. Grey slices indicate clones unique to the timepoint. White slices indicate repeating sequences isolated only once per time point. **d**, Number of nucleotide somatic hypermutations (SHM) in the *IGHV* and *IGLV* combined ($n=2050$, Supplementary Table 4) in the antibodies illustrated in **c** and Extended Data Fig. 3, compared to the number of mutations obtained after 1.3³ or 6.2⁷ months after infection (grey). Horizontal bars and red numbers indicate mean value at each time point. Samples without a prime value are shown in black. Statistical significance in **a**, **b**, and **d** was determined by two-tailed Kruskal Wallis test with subsequent Dunn’s multiple comparisons.

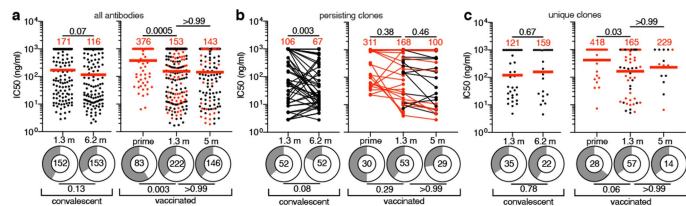


Fig. 3 | Anti-SARS-CoV-2 RBD monoclonal antibodies. **a-c.** Graphs show anti-SARS-CoV-2 neutralizing activity of monoclonal antibodies measured by a SARS-CoV-2 pseudotype virus neutralization assay using wild-type (Wuhan Hu-1⁵⁰) SARS-CoV-2 pseudovirus^{3,8}. Half-maximal inhibitory concentration (IC₅₀) values for all antibodies (**a**), persisting clones (**b**), and unique clones (**c**) isolated from convalescent individuals 1.3³ and 6.2⁷ months after infection or from vaccinated individuals after prime, and 1.3- or 5-months post-boost. Each dot represents one antibody, where 451 total antibodies were tested including the 430 reported herein (Supplementary Table 5), and 21 previously reported antibodies¹³. Antibodies isolated from samples without a prime value are shown in black. Pie charts illustrate the fraction of non-neutralizing (IC₅₀>1000 ng/ml) antibodies (grey slices), inner circle shows the number of antibodies tested per group. Horizontal bars and red numbers indicate geometric mean values. Statistical significance was determined by two-tailed Kruskal Wallis test with subsequent Dunn's multiple comparisons, and for ring plots by two-tailed Fisher's exact test with subsequent Bonferroni-correction. All experiments were performed at least twice.

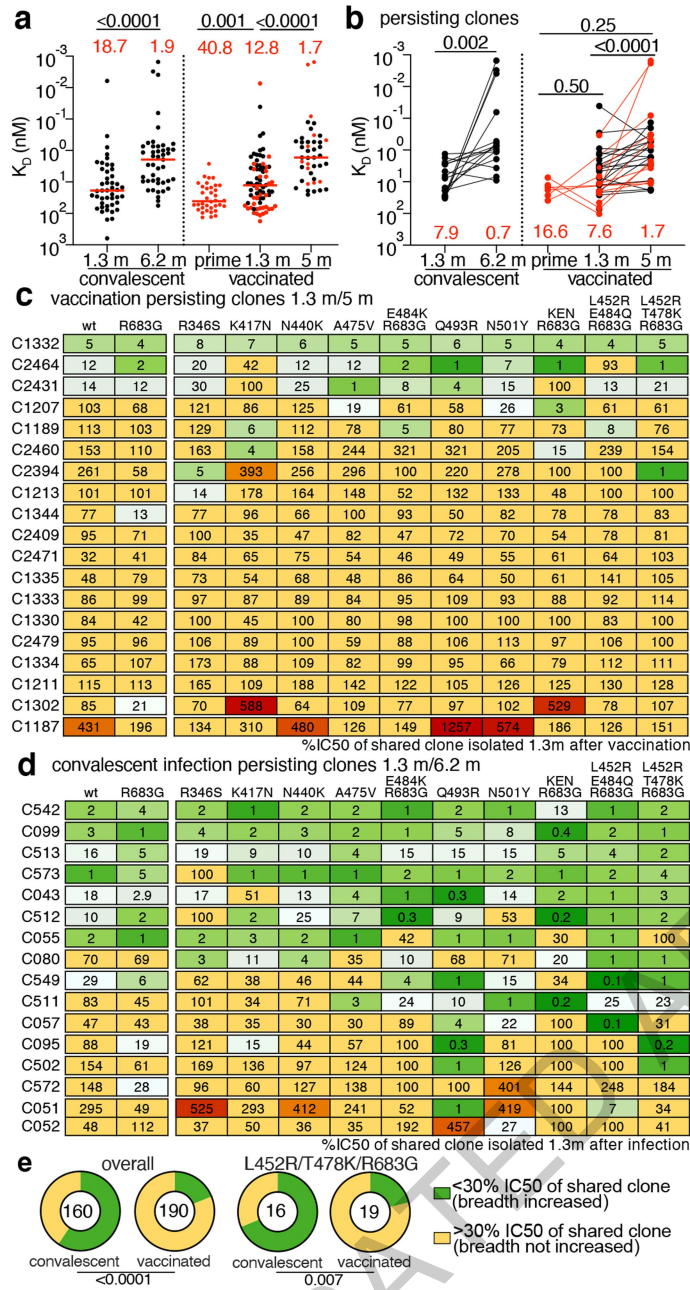


Fig. 4 | Affinity and Breadth. **a, b**, Graphs show antibody K_D s for Wuhan-Hu RBD measured by BLI. **a**, antibodies isolated from convalescent individuals 1.3³- (n=42) and 6.2-months⁷ (n=45) after infection or from vaccinees after prime (n=36), and 1.3- (n=74) and 5-months (n=43) post-second vaccination. **b**, Clonally-paired antibodies isolated from convalescent individuals 1.3³- and 6.2⁷-months after infection (n=15) or vaccinated individuals between prime and 1.3 month (n=3), prime and 5 months (n=3), or 1.3- and 5-months after full vaccination (n=26). Antibodies isolated from samples without a prime value are shown in black. Red horizontal bars and numbers indicate median values. **c, d**, Heat-maps show inhibitory concentrations of antibodies isolated 5m after vaccination (c) or 6.2m⁷ after infection (d) normalized to their shared clone isolated 1.3m after vaccination (c) or 1.3m³ after infection (d), expressed as %IC₅₀, against indicated mutant SARS-CoV-2 pseudoviruses (Supplementary Table 8). Antibodies with improved (<30%) IC₅₀ compared to their clonal relative isolated at an earlier timepoint are colored in shades of green with most improved antibodies in darkest green. Antibodies with worse (>300%) IC₅₀ than their clonal relative isolated at an earlier timepoint are colored in red with the most worsened antibodies in dark red. Antibodies that did not change their IC₅₀ by more than -3-fold are shown in yellow. **e**, Pie charts illustrate the fraction of antibodies showing improved (<30%, green) vs. not improved (yellow) IC₅₀ compared to their clonal relative isolated at an earlier timepoint. Inner circle shows the number of antibody-mutant combinations analyzed per group. Statistical significance in **a** and **b** was determined using two-tailed Kruskal Wallis test with subsequent Dunn's multiple comparisons, and in **e** by two-tailed Fisher's exact test with subsequent Bonferroni-correction.

Methods

Study participants

Participants were healthy volunteers receiving either the Moderna (mRNA-1273) or Pfizer-BioNTech (BNT162b2) mRNA vaccines against severe acute respiratory syndrome coronavirus 2 (SARS-CoV-2) who were recruited for serial blood donations at Rockefeller University Hospital in New York between January 21 and July 20, 2021. The majority of participants (n=28) were *de novo* recruited for this study, while a subgroup of individuals (n=4) were from a long-term study cohort¹³. Eligible participants were healthy adults with no history of infection with SARS-CoV-2, as determined by clinical history and confirmed through serology testing, receiving one of the two Moderna (mRNA-1273) or Pfizer-BioNTech (BNT162b2), according to current dosing and interval guidelines. Exclusion criteria included incomplete vaccination status, presence of clinical signs and symptoms suggestive of acute infection with or a positive reverse transcription polymerase chain reaction (RT-PCR) results for SARS-CoV-2 in saliva, or a positive (coronavirus disease 2019) COVID-19 serology. Seronegativity for COVID-19 was established through the absence of serological activity toward the nucleocapsid protein (N) of SARS-CoV-2. Participants presented to the Rockefeller University Hospital for blood sample collection and were asked to provide details of their vaccination regimen, possible side effects, comorbidities and possible COVID-19 history. Clinical data collection and management were carried out using the software iRIS by iMedRIS (v. 11.02). All participants provided written informed consent before participation in the study and the study was conducted in accordance with Good Clinical Practice. The study was performed in compliance with all relevant ethical regulations and the protocol (DRO-1006) for studies with human participants was approved by the Institutional Review Board of the Rockefeller University. For detailed participant characteristics see Supplementary Tables 1 and 2.

Blood samples processing and storage

Peripheral Blood Mononuclear Cells (PBMCs) obtained from samples collected at Rockefeller University were purified as previously reported by gradient centrifugation and stored in liquid nitrogen in the presence of Fetal Calf Serum (FCS) and Dimethylsulfoxide (DMSO)³⁷. Heparinized plasma and serum samples were aliquoted and stored at -20 °C or less. Prior to experiments, aliquots of plasma samples were heat-inactivated (56 °C for 1 hour) and then stored at 4 °C.

ELISAs

Enzyme-Linked Immunosorbent Assays (ELISAs)^{51,52} to evaluate antibodies binding to SARS-CoV-2 RBD were performed by coating of high-binding 96-half-well plates (Corning 3690) with 50 µl per well of a 1 µg/ml protein solution in Phosphate-buffered Saline (PBS) overnight at 4 °C. Plates were washed 6 times with washing buffer (1× PBS with 0.05% Tween-20 (Sigma-Aldrich)) and incubated with 170 µl per well blocking buffer (1× PBS with 2% BSA and 0.05% Tween-20 (Sigma)) for 1 hour at room temperature. Immediately after blocking, monoclonal antibodies or plasma samples were added in PBS and incubated for 1 hour at room temperature. Plasma samples were assayed at a 1:66 starting dilution and 10 additional threefold serial dilutions. Monoclonal antibodies were tested at 10 µg/ml starting concentration and 10 additional fourfold serial dilutions. Plates were washed 6 times with washing buffer and then incubated with anti-human IgG, IgM or IgA secondary antibody conjugated to horseradish peroxidase (HRP) (Jackson Immuno Research 109-036-088 109-035-129 and Sigma A0295) in blocking buffer at a 1:5,000 dilution (IgM and IgG) or 1:3,000 dilution (IgA). Plates were developed by addition of the HRP substrate, 3,3',5,5'-Tetramethylbenzidine (TMB) (ThermoFisher) for 10 minutes (plasma samples) or 4 minutes (monoclonal antibodies). The developing reaction was stopped by adding 50 µl of 1M H₂SO₄ and absorbance

was measured at 450 nm with an ELISA microplate reader (FluoStar Omega, BMG Labtech) with Omega and Omega MARS software for analysis. For plasma samples, a positive control (plasma from participant COV72, diluted 66.6-fold and ten additional threefold serial dilutions in PBS) was added to every assay plate for normalization. The average of its signal was used for normalization of all the other values on the same plate with Excel software before calculating the area under the curve using Prism V9.1 (GraphPad). Negative controls of pre-pandemic plasma samples from healthy donors were used for validation (for more details please see³). For monoclonal antibodies, the ELISA half-maximal concentration (EC50) was determined using four-parameter nonlinear regression (GraphPad Prism V9.1). EC50s above 2000 ng/mL were considered non-binders.

Proteins

The mammalian expression vector encoding the Receptor Binding-Domain (RBD) of SARS-CoV-2 (GenBank MN985325.1; Spike (S) protein residues 319-539) was previously described⁵³.

SARS-CoV-2 pseudotyped reporter virus

A panel of plasmids expressing RBD-mutant SARS-CoV-2 spike proteins in the context of pSARS-CoV-2-S_{Δ19} has been described^{13,25,54}. Variant pseudoviruses resembling variants of interest/concern B.1.1.7 (first isolated in the UK), B.1.351 (first isolated in South-Africa), B.1.526 (first isolated in New York City), P.1 (first isolated in Brazil) and B.1.617.2 (first isolated in India) were generated by introduction of substitutions using synthetic gene fragments (IDT) or overlap extension PCR mediated mutagenesis and Gibson assembly. Specifically, the variant-specific deletions and substitutions introduced were:

B.1.1.7: ΔH69/V70, ΔY144, N501Y, A470D, D614G, P681H, T76I, S982A, D118H

B.1.351: D80A, D215G, L242H, R246I, K417N, E484K, N501Y, D614G, A701V

B.1.526: L5F, T95I, D253G, E484K, D614G, A701V.

P.1: L18F, T20N, P26S, D138Y, R190S, K417T, E484K, N501Y, D614G, H655Y, T1027I, V1167F

B.1.617.2: T19R, Δ156-158, L452R, T478K, D614G, P681R, D950N

The E484K, K417N/E484K/N501Y, L452R/E484Q and L452R/T478K substitution, as well as the deletions/substitutions corresponding to variants of concern listed above were incorporated into a spike protein that also includes the R683G substitution, which disrupts the furin cleavage site and increases particle infectivity. Neutralizing activity against mutant pseudoviruses were compared to a wildtype (WT) SARS-CoV-2 spike sequence (NC_045512), carrying R683G where appropriate.

SARS-CoV-2 pseudotyped particles were generated as previously described^{3,8}. Briefly, 293T (CRL-11268) and HT1080 (CCL-121) cells were obtained from ATCC, and the cells were transfected with pNL4-3ΔEnv-nanoluc and pSARS-CoV-2-S_{Δ19}, particles were harvested 48 hours post-transfection, filtered and stored at -80 °C to propagate 293T/ACE2 and HT1080/AC2.cl14 cells. Cells lines were checked for mycoplasma contamination by Hoeschst staining, and confirmed negative.

Pseudotyped virus neutralization assay

Fourfold serially diluted pre-pandemic negative control plasma from healthy donors, plasma from COVID-19-convalescent individuals or monoclonal antibodies were incubated with SARS-CoV-2 pseudotyped virus for 1 hour at 37 °C. The mixture was subsequently incubated with 293T_{ACE2} cells³ (for all WT neutralization assays) or HT1080ACE2 cl14 (for all mutant panels and variant neutralization assays) cells¹³ for 48 hours after which cells were washed with PBS and lysed with Luciferase Cell Culture Lysis 5× reagent (Promega). Nanoluc Luciferase activity in lysates was measured using the Nano-Glo Luciferase Assay System (Promega) with the Glomax Navigator (Promega). The

Article

relative luminescence units were normalized to those derived from cells infected with SARS-CoV-2 pseudotyped virus in the absence of plasma or monoclonal antibodies. The half-maximal neutralization titers for plasma (NT₅₀) or half-maximal and 90% inhibitory concentrations for monoclonal antibodies (IC₅₀ and IC₉₀) were determined using four-parameter nonlinear regression (least squares regression method without weighting; constraints: top=1, bottom=0) (GraphPad Prism).

Biotinylation of viral protein for use in flow cytometry

Purified and Avi-tagged SARS-CoV-2 RBD or SARS-CoV-2 RBD K417N/E484K/N501Y mutant was biotinylated using the Biotin-Protein Ligase-BIRA kit according to manufacturer's instructions (Avidity) as described before³. Ovalbumin (Sigma, A5503-1G) was biotinylated using the EZ-Link Sulfo-NHS-LC-Biotinylation kit according to the manufacturer's instructions (Thermo Scientific). Biotinylated ovalbumin was conjugated to streptavidin-BV711 (BD biosciences, 563262) and RBD to streptavidin-PE (BD Biosciences, 554061) and streptavidin-AF647 (Biolegend, 405237)³.

Flow cytometry and single cell sorting

Single-cell sorting by flow cytometry was described previously³. Briefly, peripheral blood mononuclear cells were enriched for B cells by negative selection using a pan-B-cell isolation kit according to the manufacturer's instructions (Miltenyi Biotec, 130-101-638). The enriched B cells were incubated in Fluorescence-Activated Cell-sorting (FACS) buffer (1× PBS, 2% FCS, 1 mM ethylenediaminetetraacetic acid (EDTA)) with the following anti-human antibodies (all at 1:200 dilution): anti-CD20-PECy7 (BD Biosciences, 335793), anti-CD3-APC-eFluor 780 (Invitrogen, 47-0037-41), anti-CD8-APC-eFluor 780 (Invitrogen, 47-0086-42), anti-CD16-APC-eFluor 780 (Invitrogen, 47-0168-41), anti-CD14-APC-eFluor 780 (Invitrogen, 47-0149-42), as well as Zombie NIR (BioLegend, 423105) and fluorophore-labeled RBD and ovalbumin (Ova) for 30 min on ice. Single CD3-CD8-CD14-CD16-CD20+Ova-RBD-PE+RBD-AF647+ B cells were sorted into individual wells of 96-well plates containing 4 μl of lysis buffer (0.5× PBS, 10 mM Dithiothreitol (DTT), 3,000 units/ml RNasin Ribonuclease Inhibitors (Promega, N2615) per well using a FACS Aria III and FACSDiva software (Becton Dickinson) for acquisition and FlowJo for analysis. The sorted cells were frozen on dry ice, and then stored at -80 °C or immediately used for subsequent RNA reverse transcription. For plasmablast single-cell sorting, in addition to above antibodies, B cells were also stained with anti-CD19-BV605 (Biolegend, 302244), and single CD3-CD8-CD14-CD16-CD19+CD20-Ova-RBD-PE+RBD-AF647+ plasmablasts were sorted as described above. For B cell phenotype analysis, in addition to above antibodies, B cells were also stained with following anti-human antibodies (all at 1:200 dilution): anti-IgD-BV421 (Biolegend, 348226), anti-CD27-FITC (BD biosciences, 555440), anti-CD19-BV605 (Biolegend, 302244), anti-CD71-PerCP-Cy5.5 (Biolegend, 334114), anti-IgG-PECF594 (BD biosciences, 562538), anti-IgM-AF700 (Biolegend, 314538), anti-IgA-Viogreen (Miltenyi Biotec, 130-113-481).

Antibody sequencing, cloning and expression

Antibodies were identified and sequenced as described previously^{3,55}. In brief, RNA from single cells was reverse-transcribed (SuperScript III Reverse Transcriptase, Invitrogen, 18080-044) and the cDNA was stored at -20 °C or used for subsequent amplification of the variable IGH, IGL and IGK genes by nested PCR and Sanger sequencing. Sequence analysis was performed using MacVector. Amplicons from the first PCR reaction were used as templates for sequence- and ligation-independent cloning into antibody expression vectors. Recombinant monoclonal antibodies were produced and purified as previously described³.

Biolayer interferometry

Biolayer interferometry assays were performed as previously described³. Briefly, we used the Octet Red instrument (ForteBio) at 30 °C

with shaking at 1,000 r.p.m. Affinity measurement of anti-SARS-CoV-2 IgGs binding were corrected by subtracting the signal obtained from traces performed with IgGs in the absence of WT RBD. The kinetic analysis using protein A biosensor (ForteBio 18-5010) was performed as follows: (1) baseline: 60sec immersion in buffer. (2) loading: 200sec immersion in a solution with IgGs 10 μg/ml. (3) baseline: 200sec immersion in buffer. (4) Association: 300sec immersion in solution with WT RBD at 20, 10 or 5 μg/ml (5) dissociation: 600sec immersion in buffer. Curve fitting was performed using a fast 1:1 binding model and the Data analysis software (ForteBio). Mean equilibrium dissociation constant (K_d) values were determined by averaging all binding curves that matched the theoretical fit with an R² value ≥ 0.8.

Computational analyses of antibody sequences

Antibody sequences were trimmed based on quality and annotated using Igbblastn v.1.14. with IMGT domain delineation system. Annotation was performed systematically using Change-O toolkit v.0.4.540⁵⁶. Heavy and light chains derived from the same cell were paired, and clonotypes were assigned based on their V and J genes using in-house R and Perl scripts. All scripts and the data used to process antibody sequences are publicly available on GitHub (https://github.com/stratust/igppipeline/tree/igppipeline2_timepoint_v2).

The frequency distributions of human V genes in anti-SARS-CoV-2 antibodies from this study was compared to 131,284,220 IgH and IGL sequences generated by⁵⁷ and downloaded from cAb-Rep⁵⁸, a database of human shared BCR clonotypes available at <https://cab-rep.c2b2.columbia.edu/>. Based on the 112 distinct V genes that make up the 7936 analyzed sequences from Ig repertoire of the 11 participants present in this study, we selected the IgH and IGL sequences from the database that are partially coded by the same V genes and counted them according to the constant region. The frequencies shown in Extended Data Fig. 4 are relative to the source and isotype analyzed. We used the two-sided binomial test to check whether the number of sequences belonging to a specific *IGHV* or *IGLV* gene in the repertoire is different according to the frequency of the same IgV gene in the database. Adjusted p-values were calculated using the false discovery rate (FDR) correction. Significant differences are denoted with stars.

Nucleotide somatic hypermutation and Complementarity-Determining Region (CDR3) length were determined using in-house R and Perl scripts. For somatic hypermutations, *IGHV* and *IGLV* nucleotide sequences were aligned against their closest germlines using Igbblastn and the number of differences were considered nucleotide mutations. The average number of mutations for V genes was calculated by dividing the sum of all nucleotide mutations across all participants by the number of sequences used for the analysis.

Data presentation

Figures arranged in Adobe Illustrator 2020.

Reporting summary

Further information on research design is available in the Nature Research Reporting Summary linked to this paper.

Data availability

Data are provided in Supplementary Tables 1–8. The raw sequencing data and computer scripts associated with Fig. 2 and Extended Data Fig. 3 have been deposited at Github (https://github.com/stratust/igppipeline/tree/igppipeline2_timepoint_v2). This study also uses data from “A Public Database of Memory and Naive B-Cell Receptor Sequences” (<https://doi.org/10.5061/dryad.35ks2>), PDB (6VYB and 6NB6), cAb-Rep (<https://cab-rep.c2b2.columbia.edu/>), Sequence Read Archive (accession SRP010970), and from “High frequency of shared clonotypes in human B cell receptor repertoires” (<https://doi.org/10.1038/s41586-019-0934-8>).

Code availability

Computer code to process the antibody sequences is available at GitHub (https://github.com/stratust/igpipeline/tree/igpipeline2_timepoint_v2).

51. Amanat, F. et al. A serological assay to detect SARS-CoV-2 seroconversion in humans. *Nat. Med.* **26**, 1033-1036, <https://doi.org/10.1038/s41591-020-0913-5> (2020).
52. Grifoni, A. et al. Targets of T Cell Responses to SARS-CoV-2 Coronavirus in Humans with COVID-19 Disease and Unexposed Individuals. *Cell* **181**, 1489-1501 e1415, <https://doi.org/10.1016/j.cell.2020.05.015> (2020).
53. Barnes, C. O. et al. Structures of Human Antibodies Bound to SARS-CoV-2 Spike Reveal Common Epitopes and Recurrent Features of Antibodies. *Cell* **182**, 828-842 e816, <https://doi.org/10.1016/j.cell.2020.06.025> (2020).
54. Weisblum, Y. et al. Escape from neutralizing antibodies by SARS-CoV-2 spike protein variants. *Elife* **9**, <https://doi.org/10.7554/eLife.61312> (2020).
55. Wang, Z. et al. Enhanced SARS-CoV-2 neutralization by dimeric IgA. *Sci Transl Med* **13**, <https://doi.org/10.1126/scitranslmed.abf1555> (2021).
56. Gupta, N. T. et al. Change-O: a toolkit for analyzing large-scale B cell immunoglobulin repertoire sequencing data. *Bioinformatics* **31**, 3356-3358, <https://doi.org/10.1093/bioinformatics/btv359> (2015).
57. Soto, C. et al. High frequency of shared clonotypes in human B cell receptor repertoires. *Nature* **566**, 398-402, <https://doi.org/10.1038/s41586-019-0934-8> (2019).
58. Guo, Y., Chen, K., Kwong, P. D., Shapiro, L. & Sheng, Z. cAb-Rep: A Database of Curated Antibody Repertoires for Exploring Antibody Diversity and Predicting Antibody Prevalence. *Front Immunol* **10**, 2365, <https://doi.org/10.3389/fimmu.2019.02365> (2019).

Acknowledgements We thank all study participants who devoted time to our research; The Rockefeller University Hospital nursing staff and Clinical Research Support Office and nursing

staff. Mayu Okawa Frank, Marissa Bergh, and Robert B. Darnell for SARS-CoV-2 saliva PCR testing. Charles M. Rice, and all members of the M.C.N. laboratory for helpful discussions, Maša Jankovic for laboratory support, and Kristie Gordon for technical assistance with cell-sorting experiments. This work was supported by NIH grant P01-AI138398-S1 (M.C.N.) and 2U19AI111825 (M.C.N.). R37-AI64003 to P.D.B.; R01AI78788 to T.H. F.M. is supported by the Bulgari Women & Science Fellowship in COVID-19 Research. C.G. was supported by the Robert S. Wennett Post-Doctoral Fellowship. D.S.B. and C.G. were supported in part by the National Center for Advancing Translational Sciences (National Institutes of Health Clinical and Translational Science Award program, grant UL1 TR001866), and C.G. by the Shapiro-Silverberg Fund for the Advancement of Translational Research. P.D.B. and M.C.N. are Howard Hughes Medical Institute Investigators.

Author contributions P.D.B., T.H., and M.C.N. conceived, designed and analyzed the experiments. M. Caskey and C.G. designed clinical protocols. A.C, F.M., D.S.B., Z.W., S.F., P.M., M.A., E.B., J.D.S., I.S., J.D. F.S., F.Z., T.B.T., AND M.J. carried out experiments. A.G. and M. Cipolla produced antibodies. D.S.B., M.D., M.T., K.G.M., C.G. and M. Caskey recruited participants, executed clinical protocols. T.Y.O. and V.R. performed bioinformatic analysis. A.C., F.M, D.S.B., Z.W., S.F., and M.C.N. wrote the manuscript with input from all co-authors.

Competing interests The Rockefeller University has filed a provisional patent application in connection with this work on which M.C.N. is an inventor (US patent 63/021,387). The patent has been licensed by Rockefeller University to Bristol Meyers Squibb.

Additional information

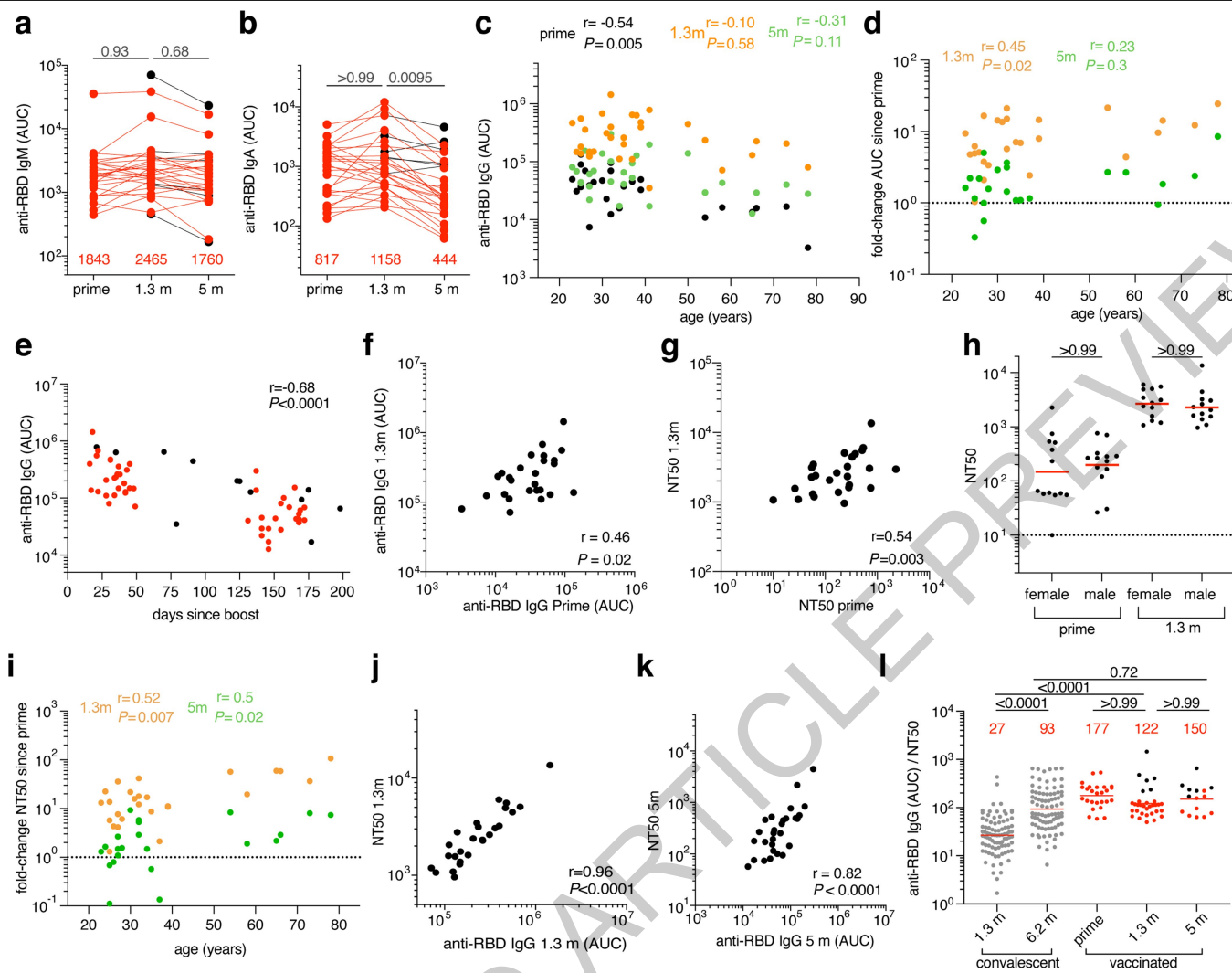
Supplementary information The online version contains supplementary material available at <https://doi.org/10.1038/s41586-021-04060-7>.

Correspondence and requests for materials should be addressed to M.C., P.D.B., T.H. or M.C.N.

Peer review information *Nature* thanks the anonymous reviewer(s) for their contribution to the peer review of this work.

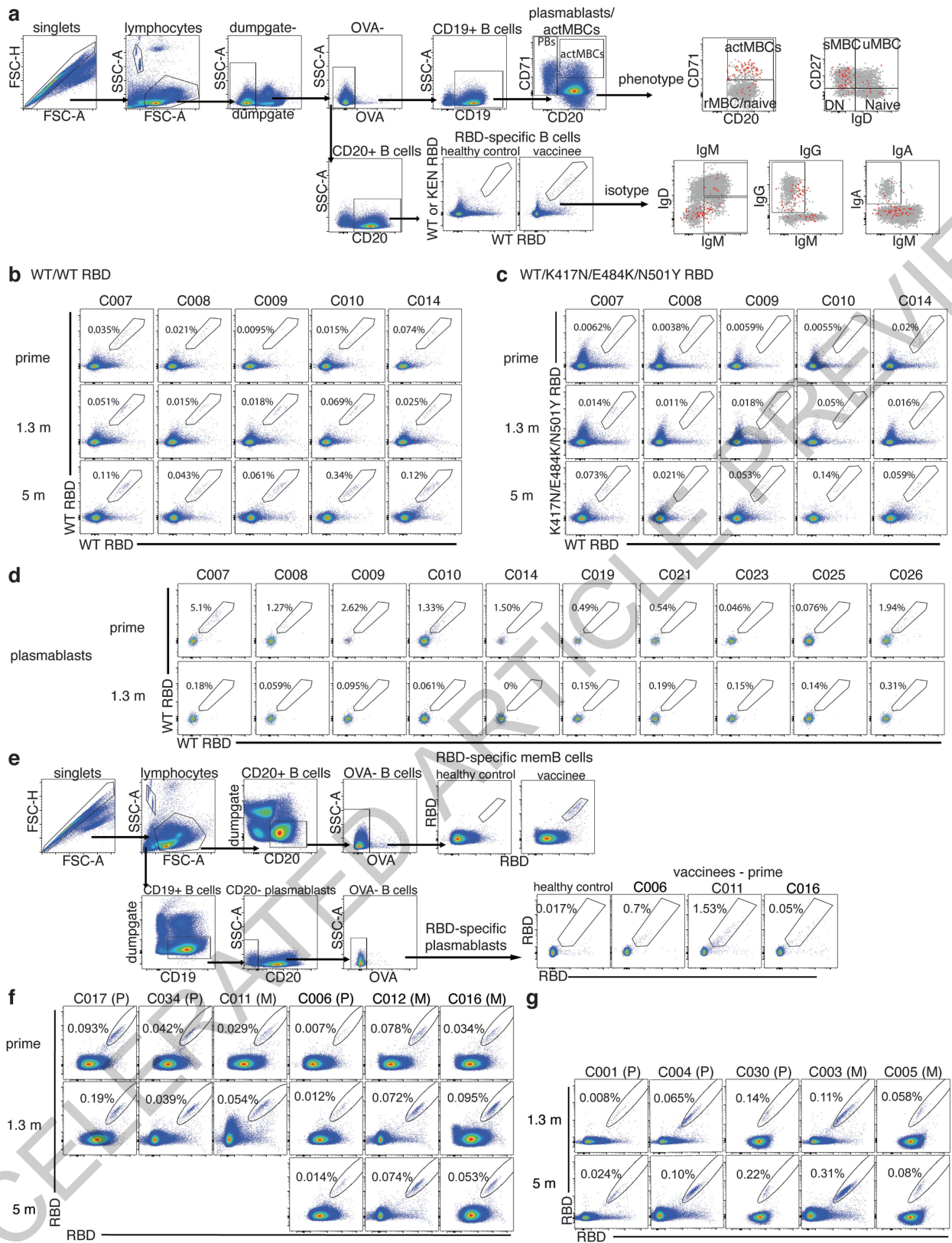
Reprints and permissions information is available at <http://www.nature.com/reprints>.

ACCELERATED ARTICLE PREVIEW



Extended Data Fig. 1 | Plasma ELISA and neutralization. **a, b**, Graph shows area under the curve (AUC, Y-axis) for plasma IgM (**a**) or IgA (**b**) antibody binding to SARS-CoV-2 RBD after prime, and 1.3- and 5-months post-boost for paired samples from $n=32$ vaccinated individuals. Samples without a prime value are shown in black. **c**, Graph shows plasma IgG antibody binding (AUC, Y-axis) plotted against age (X-axis) after prime (black), and 1.3 months (orange) and 5 months (green) post-second vaccination in $n=32$ vaccinated individuals. **d**, Graph shows age (years, X-axis) vs. fold-change of IgG-binding titers (AUC, Y-axis) between prime and 1.3m (orange) or 5m (green) post-boost in $n=32$ vaccinated individuals. **e**, Graph shows plasma IgG antibody binding AUC values (Y-axis) plotted against time after vaccination (day, X-axis) from $n=32$ vaccinated individuals. Samples without a prime value are shown in black. **f**, IgG antibody binding after prime (AUC, X-axis) vs. IgG antibody binding after 1.3 months post-boost (AUC, Y-axis) ($n=26$). **g**, NT50 values after prime (X-axis) vs. NT50 values after 1.3 months post-boost (Y-axis) in individuals receiving two doses of an mRNA vaccine ($n=26$). **h**, NT50 values after prime and 1.3 months

post-boost in females and males receiving 2 doses of an mRNA vaccine ($n=26$). **i**, Graph shows age (years, X-axis) vs fold-change of NT50 (X-axis) between prime and 1.3m (orange) or 5m (green) post-boost ($n=26$). **j**, NT50 values (Y-axis) vs. IgG antibody binding (AUC, X-axis) 1.3 months after 2 doses of an mRNA vaccine ($n=26$). **k**, NT50 values (Y-axis) vs. IgG antibody binding (AUC, X-axis) 5 months after boost in individuals receiving two doses of an mRNA vaccine ($n=28$). **l**, Ratio of anti-RBD IgG antibody (AUC) to NT50 values (Y-axis) plotted for convalescent infected individuals (grey) 1.3m³ or 6.2m⁷ after infection, and from $n=32$ vaccinated individuals after the prime, and 1.3m and 5m after receiving 2 doses of an mRNA vaccine. Samples without a prime value are shown in black. All experiments were performed at least in duplicate. Red values or bar in **a, b, h** and **l** represent geometric mean values. Statistical significance in **a, b, h**, and **l** was determined by two-tailed Kruskal-Wallis test with subsequent Dunn's multiple comparisons, or by two-tailed Spearman correlation test in **c, d, e, f, g, i, j**, and **k**.



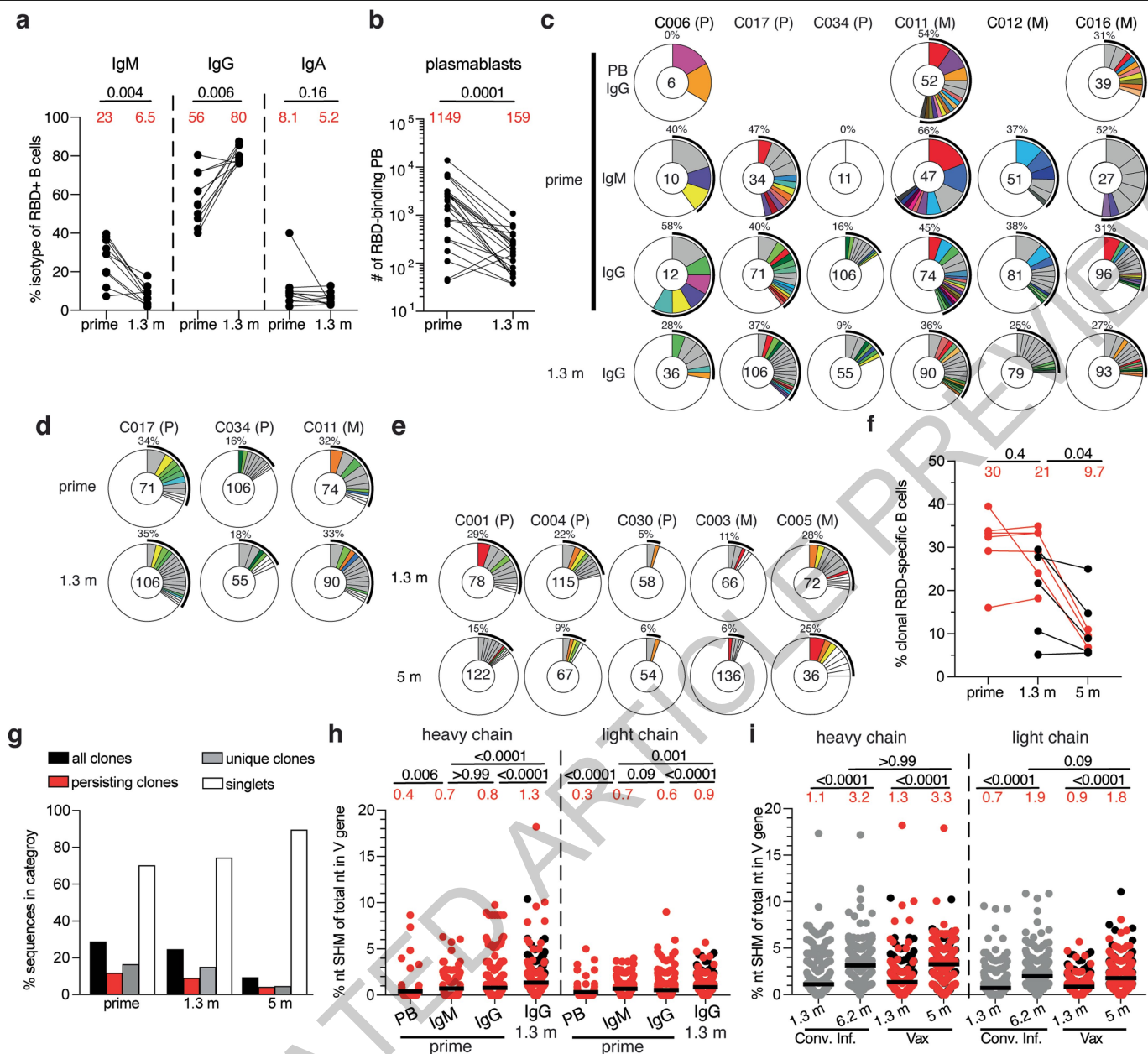
Extended Data Fig. 2 | See next page for caption.

Article

Extended Data Fig. 2 | Flow Cytometry. a, Gating strategy for phenotyping. Gating was on singlets that were CD19⁺ or CD20⁺ and CD3-CD8-CD16-Ova-. Anti-IgG, IgM, IgA, IgD, CD71 and CD27 antibodies were used for B cell phenotype analysis. Antigen-specific cells were detected based on binding to RBD WT-PE⁺ and RBD WT/KEN (K417N/E484K/N501Y)-AF647⁺. **b-c**, Flow cytometry plots showing the frequency of **b**, RBD WT-binding memory B cells, and **c**, RBD-binding memory B cells cross-reactive with WT and K417N/E484K/N501Y mutant RBD in 5 selected individuals, after prime, 1.3 months, and 5 months post-second vaccination. **d**, Flow cytometry plots showing frequency of RBD-

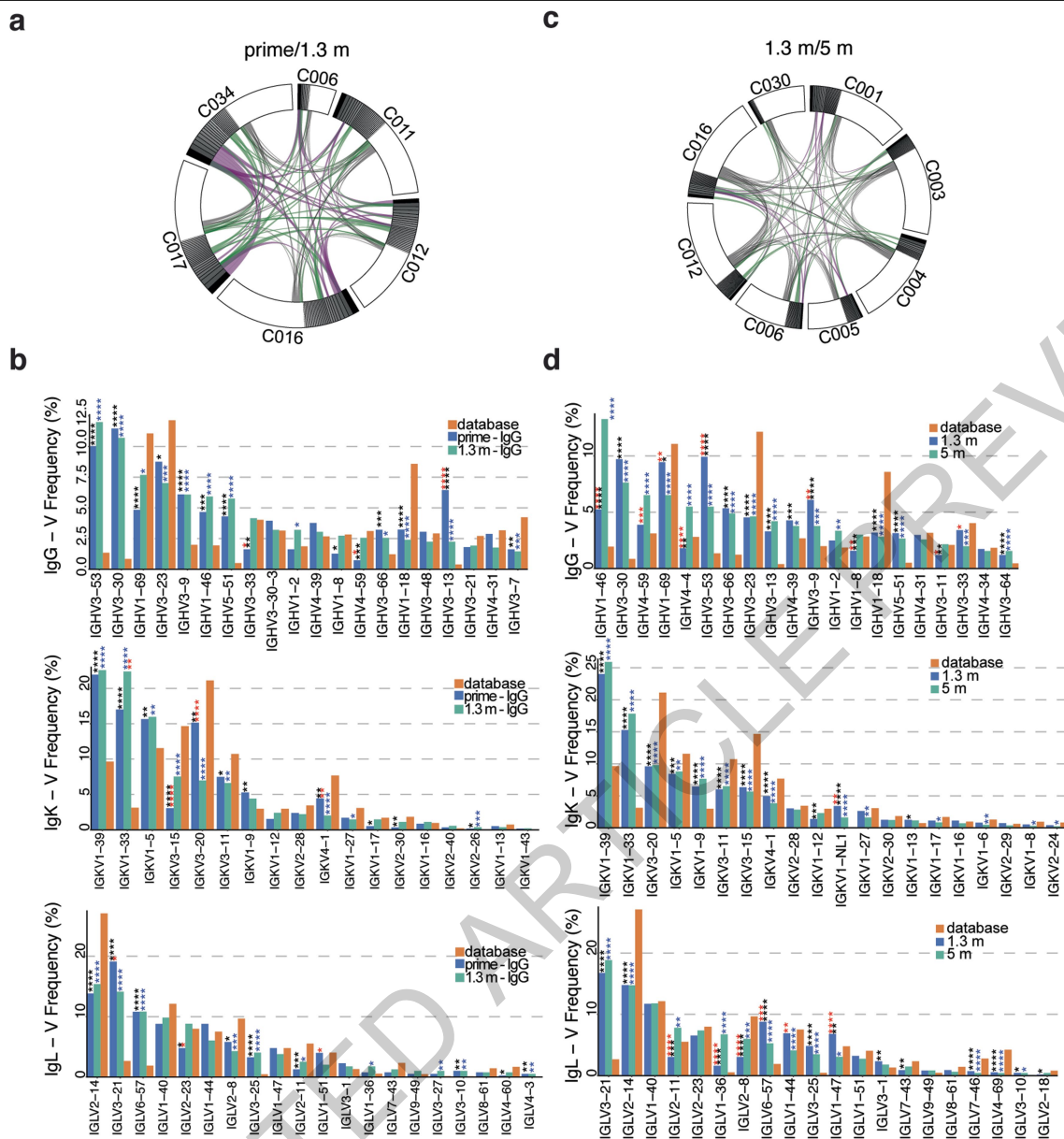
binding plasmablasts, in 10 selected vaccinees after prime or 1.3 months post-boost. **e**, Gating strategy for single-cell sorting for CD20⁺ memory B cells (top panel) or CD19⁺CD20⁻ plasmablasts (bottom panel) which were double positive for RBD-PE and RBD-AF647. **f-g**, Representative flow cytometry plots showing dual AlexaFluor-647-RBD and PE-RBD-binding, single-cell sorted B cells from **f**, 6 individuals after prime and 1.3 months or 5 months post-boost and **g**, 5 individuals from 1.3- or 5-months post-boost. Percentage of RBD-specific B cells is indicated.

ACCELERATED ARTICLE PREVIEW



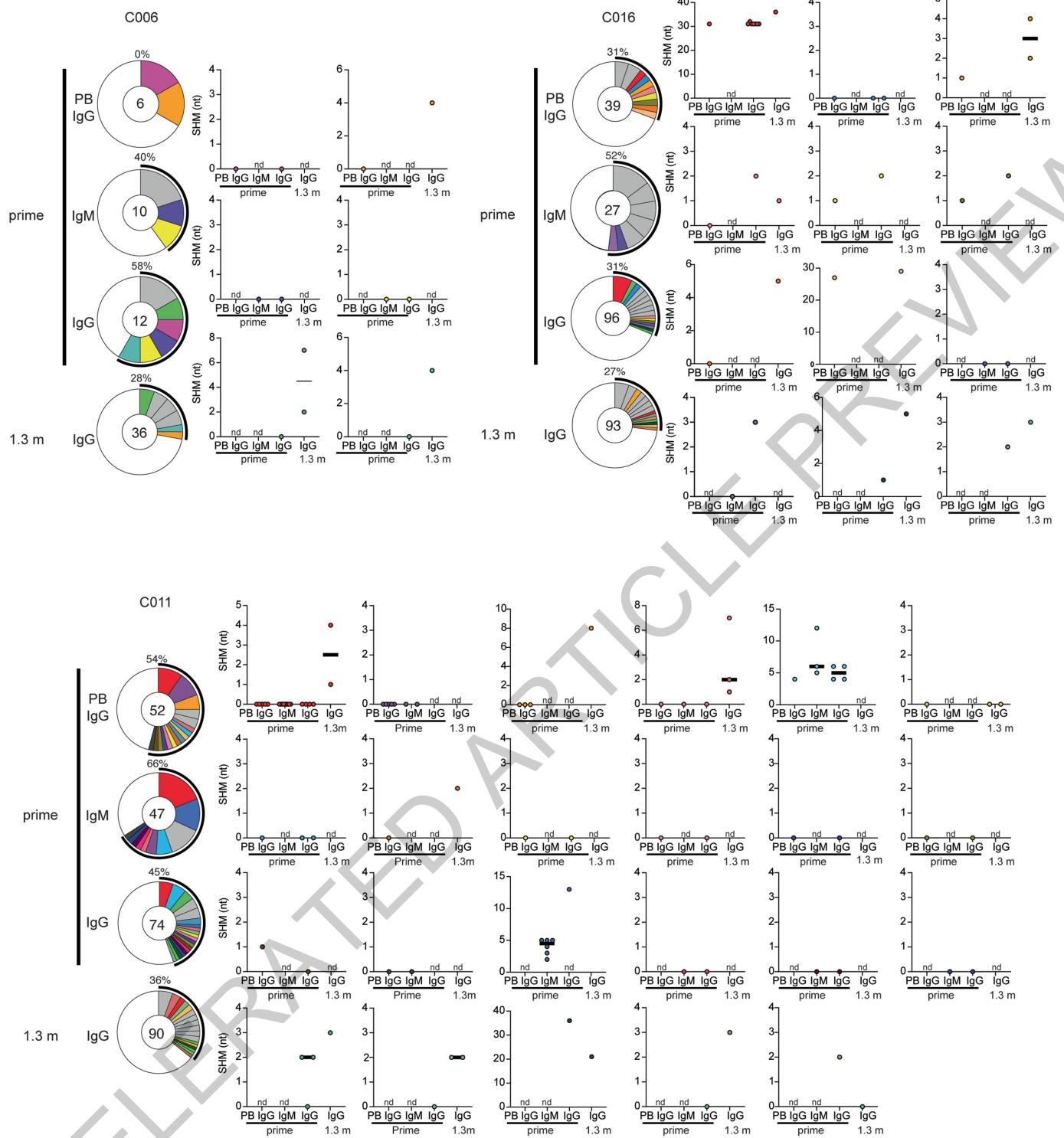
Extended Data Fig. 3 | anti-SARS-CoV-2 RBD-specific plasmablast and memory B cells responses after vaccination. a-b, Graph showing the a, frequency of IgM, IgG, or IgA isotype expression by Wuhan-Hu RBD-specific memory B cells after prime or 1.3 months post-boost ($n=10$), and b, number of Wuhan-Hu RBD-binding plasmablasts per 10 million B cells ($n=26$) after prime or 1.3 months post-boost. Red numbers indicate geometric means. Gating strategy is in Extended Data Fig. 2. **c-e,** Pie charts show the distribution of IgG antibody sequences obtained from c, 6 individuals after prime (upper panel) or 1.3 months post-boost (lower panel). The number inside the circle indicates the number of sequences analyzed for the individual denoted above the circle, with Pfizer vaccinees indicated by (P) and Moderna by (M). Pie slice size is proportional to the number of clonally related sequences. The black outline and associated numbers indicate the percentage of clonally expanded sequences detected at each time point. Colored slices indicate persisting clones (same *IGHV* and *IGLV* genes, with highly similar CDR3s) found at more than one timepoint within the same individual. Grey

slices indicate clones unique to the timepoint. White slices indicate repeating sequences isolated only once per timepoint. **f,** Graph shows the relative percentage of clonal sequences of IgG memory B cells at each time point from $n=11$ vaccinated individuals illustrated in Fig. 2c and Extended Data Fig. 3d, e. The red numbers indicate the geometric means. Samples without a prime value are shown in black. **g,** Graph shows the percentage of total paired-sequences from IgG memory B cells ($n=2050$) analyzed at either prime, 1.3- or 5-months post-boost, that can be found as part of all clones (black bars), persisting clones (red bars), unique clones (grey bars), or singlets (white bar). **h-i,** Ratio of the number of somatic nucleotide mutations over the nucleotide length of the V gene in the Ig heavy and light chains, separately, in antibodies detected in **h**, different B cell compartments after prime or 1.3 months post-boost ($n=1565$) and **i**, IgG memory B cells at 1.3 or 5 months post-boost ($n=1610$) compared to convalescent infected (grey) individuals after 1.3³ and 6.2⁷ months post-infection (also Supplementary Table 4). Horizontal bars and red numbers indicate mean ratio in each compartment at each time point. Sequences derived from samples without a prime value are shown in black. Statistical significance in **a** and **b** was determined using a two-tailed Wilcoxon matched-pairs signed rank test. **f**, **h**, and **i** was determined by two-tailed Kruskal Wallis test with subsequent Dunn's multiple comparisons.



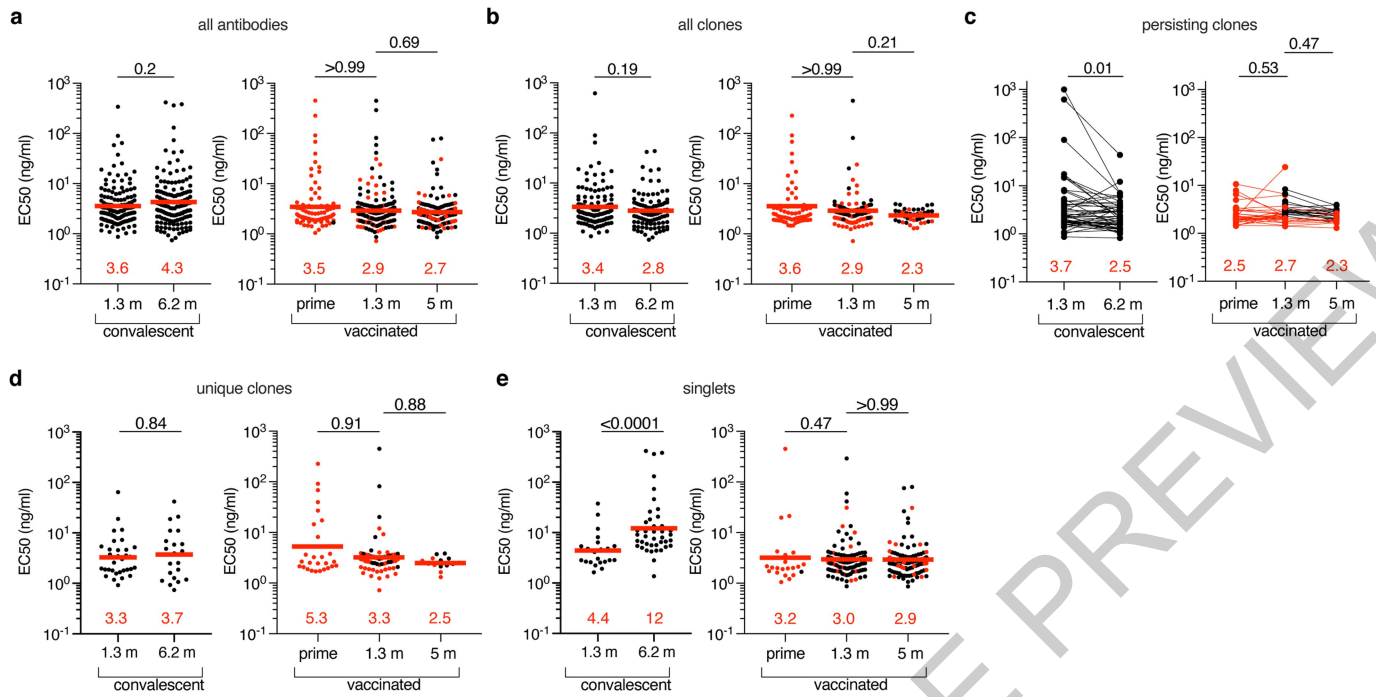
Extended Data Fig. 4 | Frequency distribution of human V genes. a, Circos plot depicting relationship between antibodies that share V and J gene usage in both IgH and IgL when comparing prime/1.3m IgG MBC sequences. Purple, green, and grey lines connect related clones, clones and singlets, and singlets to each other, respectively. **b,** Graph shows relative abundance of human heavy chain *IGHV* (top), light chain *IGKV* (middle) or *IGLV* (bottom) genes comparing Sequence Read Archive accession SRP010970 (orange), and IgG MBCs after prime (blue) or 1.3 months post-boost (green). Statistical significance was determined by two-sided binomial test. * = $p \leq 0.05$, ** = $p \leq 0.01$, *** = $p \leq 0.001$, **** = $p \leq 0.0001$. Color of stars indicates: black - comparing Database versus Prime; blue - comparing Database versus 1.3m; red - comparing Prime versus

1.3m. **c,** Circos plot depicting relationship between antibodies that share V and J gene usage in both IgH and IgL when comparing 1.3m/5m IgG MBC sequences. Purple, green, and grey lines connect related clones, clones and singlets, and singlets to each other, respectively. **d,** Graph shows relative abundance of human heavy chain *IGHV* (top), light chain *IGKV* (middle) or *IGLV* (bottom) genes comparing Sequence Read Archive accession SRP010970 (orange), and IgG MBCs after 1.3 months (blue) or 5 months (green) post-vaccination. Statistical significance was determined by two-sided binomial test. * = $p \leq 0.05$, ** = $p \leq 0.01$, *** = $p \leq 0.001$, **** = $p \leq 0.0001$. Color of stars indicates: black - comparing Database versus 1.3 months; blue - comparing Database versus 5 months; red - comparing 1.3 months versus 5 months.



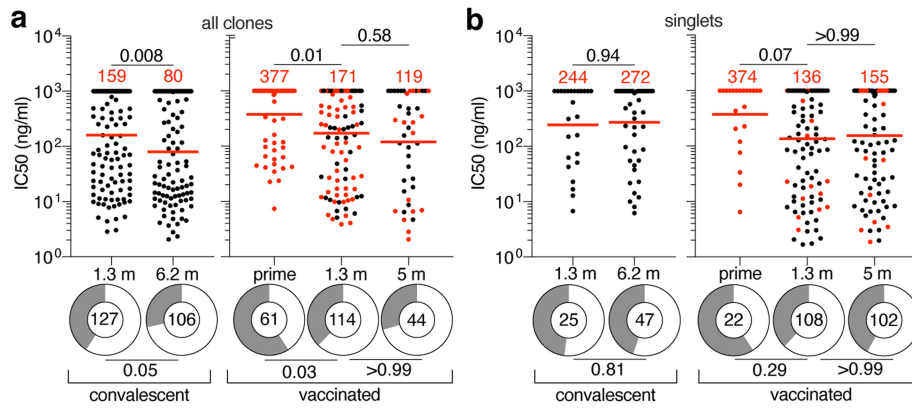
Extended Data Fig. 5 | Somatic hypermutation of anti-SARS-CoV-2 RBD antibody clones after prime or boost. Clonal evolution of RBD-binding B cells from 3 individuals for which plasmablasts, IgM memory B cells, and IgG memory B cells were analyzed after prime, and IgG memory B cells were analyzed after 1.3 months post-boost (as described in Extended Data Fig. 3).

The number of somatic nucleotide mutations found in shared clonal families found in at least 2 different compartments is graphed to the right of each donut plot. Color of dot plots match the color of pie slices within the donut plot, which indicate persisting clones. nd - clone was Not Detected in the indicated compartment. Black horizontal line indicates median number of SHM.



Extended Data Fig. 6 | Anti-SARS-CoV-2 RBD monoclonal antibodies ELISAs. **a-e**, Graphs show anti-SARS-CoV-2 binding activity of $n=458$ monoclonal antibodies measured by ELISA against RBD. ELISA half-maximal concentration (EC_{50}) values for all antibodies (**a**), all clones (**b**), persisting clones (**c**), unique clones (**d**) and singlets (**e**) isolated from COVID-19 convalescent individuals 1.3³ and 6.2⁷ months after infection (left panel) or from vaccinated individuals after prime, or 1.3m or 5m after receiving the

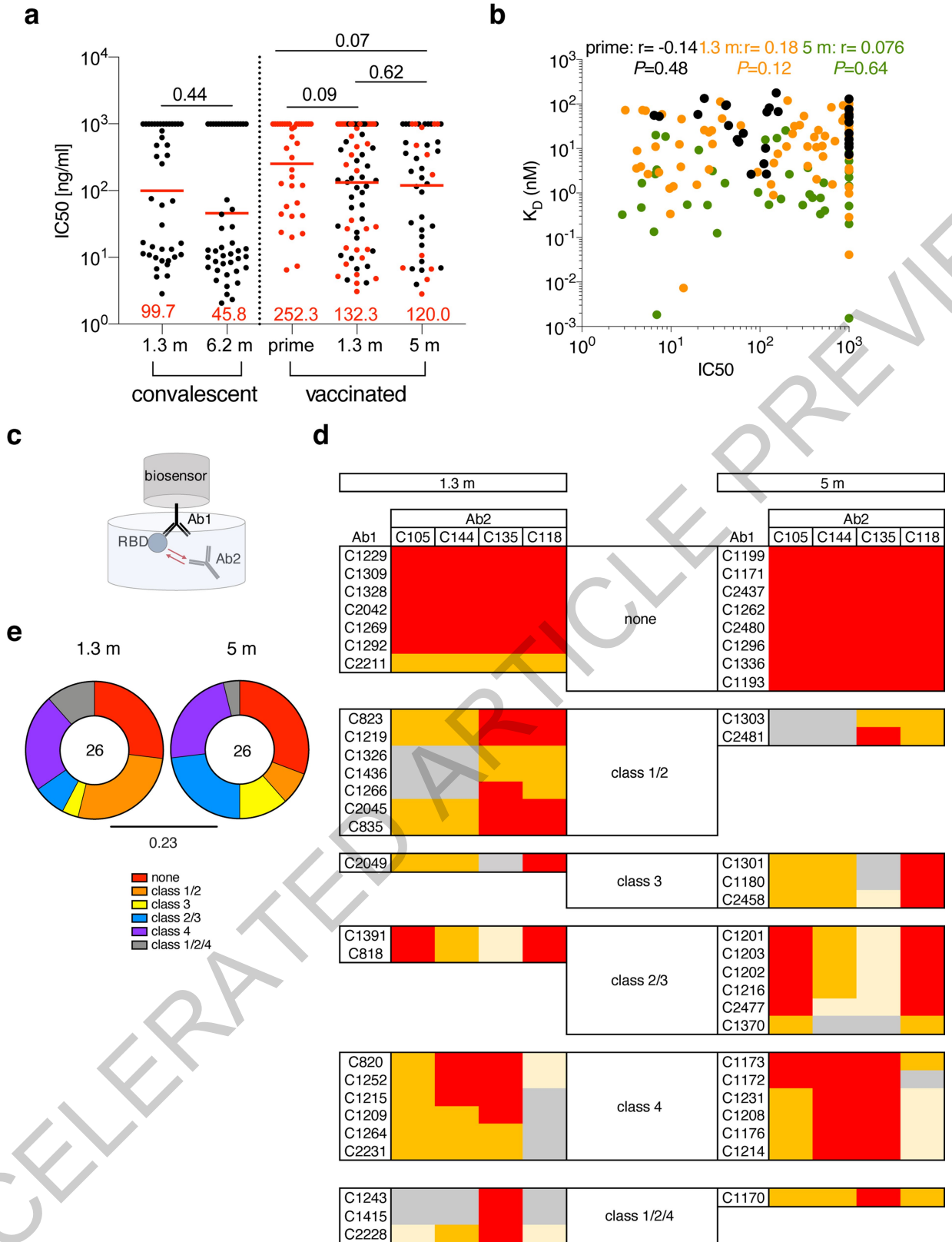
second dose of mRNA vaccination (right panel). Each dot represents one antibody. Antibodies isolated from samples without a prime value are shown in black. Red horizontal bars and numbers indicate geometric mean values. Statistical significance was determined by two-tailed Mann-Whitney test (left panels of **a**, **b**, **d** and **e**), two-tailed Kruskal-Wallis test with subsequent Dunn's multiple comparisons (right panels of **a-e**) or by two-tailed Wilcoxon test (left panel of **c**). All experiments were performed at least twice.



Extended Data Fig. 7 | Anti-SARS-CoV-2 RBD monoclonal antibodies.

a–b, Graphs show anti-SARS-CoV-2 neutralizing activity of monoclonal antibodies measured by a SARS-CoV-2 pseudotype virus neutralization assay using wild-type (Wuhan Hu-1⁵⁰) SARS-CoV-2 pseudovirus^{3,8}. Half-maximal inhibitory concentration (IC₅₀) values for antibodies from **a**, all clones and **b**, singlets isolated from COVID-19 convalescent individuals 1.3³ and 6.2⁷ months after infection or from vaccinated individuals after prime, and 1.3- or 5-months after 2 doses of vaccine. Each dot represents one antibody, where 451 total antibodies were tested including the 430 reported herein (Supplementary

Table 5), and 21 previously reported antibodies¹³. Antibodies isolated from samples without a prime value are shown in black. Pie charts illustrate the fraction of non-neutralizing (IC₅₀ > 1000 ng/ml) antibodies (grey slices), inner circle shows the number of antibodies tested per group. Horizontal bars and red numbers indicate geometric mean values. Statistical significance was determined by two-tailed Kruskal Wallis test with subsequent Dunn's multiple comparisons, and for ring plots by two-tailed Fisher's exact test with subsequent Bonferroni-correction. All experiments were performed at least twice.

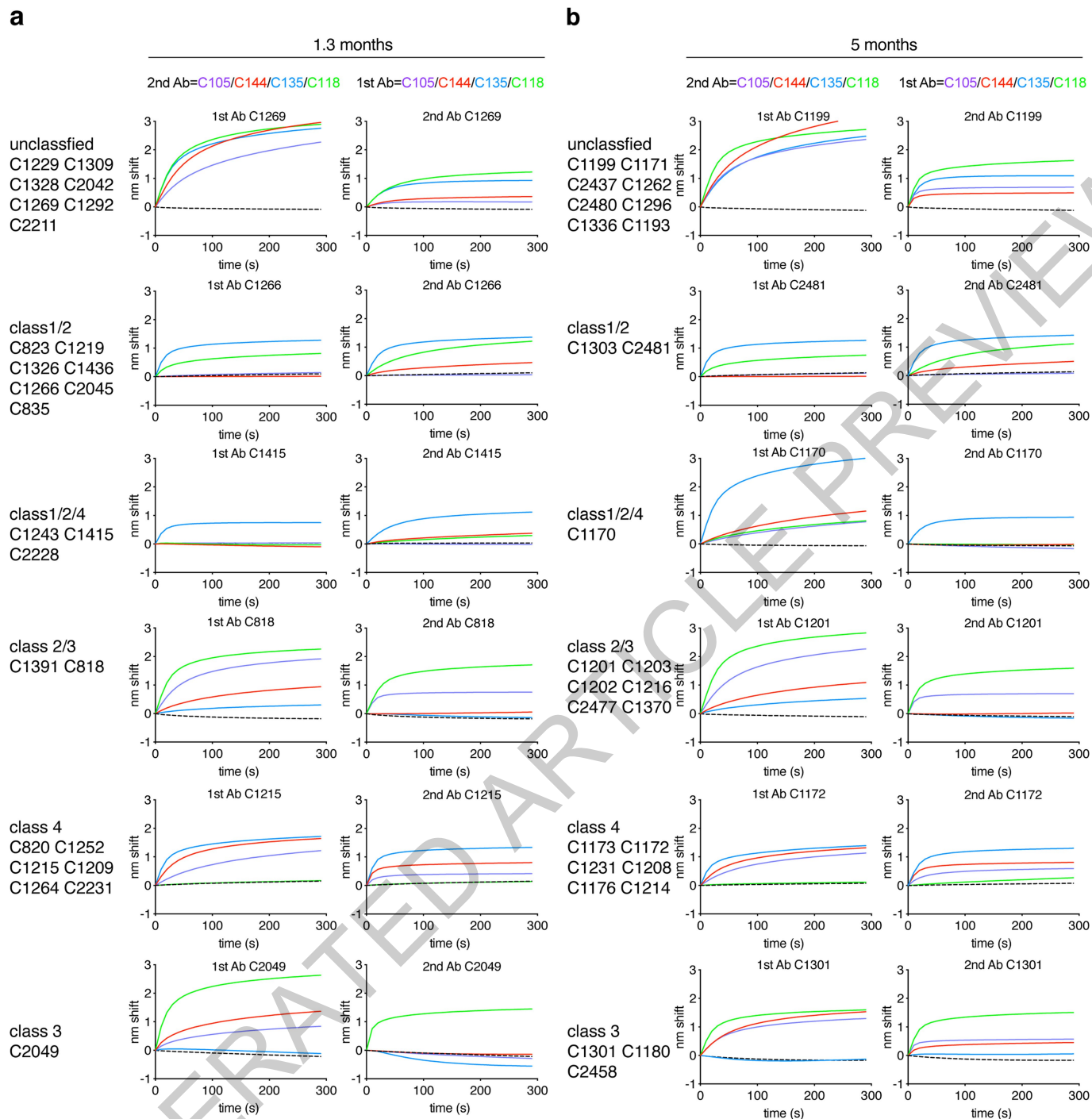


Extended Data Fig. 8 | See next page for caption.

Extended Data Fig. 8 | Affinity and Epitope targeting of anti-SARS-CoV-2 RBD antibodies. **a.** IC_{50} values for randomly selected antibodies isolated from convalescents 1.3m³ (n=42) and 6.2m⁷ (n=45) after infection or from vaccinees after prime (n=36), and 1.3m (n=74) and 5m (n=43). Red horizontal lines and numbers indicate geometric mean. Antibodies isolated from samples without a prime value are shown in black. **b.** Graphs show affinities (K_D , Y-axis) plotted against neutralization activity (IC_{50} , X-axis) for antibodies isolated after prime (black), or 1.3m (orange) or 5m (green) post-boost vaccination for antibodies shown in **a.** **c.** Schematic representation of the BLI experiment for randomly selected antibodies isolated from vaccinees 1.3- and 5 months after full vaccination (each presented group shows n=26 antibodies). **d.** Heat-map of

relative inhibition of Ab2 binding to the preformed Ab1-RBD complexes (grey=no binding, yellow=low binding, orange=intermediate binding, red=high binding). Values are normalized through the subtraction of the autologous antibody control. BLI traces can be found in Extended Data Fig. 9. **e.** Pie charts indicate the fraction of antibodies that are assigned to different classes according to their binding pattern as shown in **d** and Extended data Fig. 9. Number in inner circle shows number of antibodies tested. Statistical significance was determined using a two-tailed Kruskal Wallis test with subsequent Dunn's multiple comparisons in **a** and two-tailed Spearman correlation test in **b**, and a two-tailed Chi-square test in **e**.

ACCELERATED ARTICLE PREVIEW



Extended Data Fig. 9 | BLI traces from epitope mapping of anti-SARS-CoV-2 RBD antibodies. a, b, BLI traces from competition experiments used to determine epitope targets of anti-SARS-CoV-2 RBD antibodies isolated from vaccinees at 1.3m (a) or 5m (b) post-boost, as illustrated in Extended Data Fig. 8.

Extended Data Table 1 | Breadth of anti-SARS-CoV-2 RBD antibodies elicited after prime and 2 doses of vaccination

a

	wt		R683G		R346S		K417N		N440K		A475V		E484K		Q493R		N501Y		KEN		L452R		
C2159	12.2	6.2	9.1	3.3	11.2	8.8	627.1	17.1	20.6	212.0	36.9												
C2029	25.1	7.6	>1000	5.9	23.0	19.5	1.8	14.6	57.7	1.6	>1000												
C2139	46.0	25.4	33.0	>1000	48.7	>1000	153.6	>1000	>1000	>1000	105.1												
C2033	46.2	25.8	32.0	>1000	41.4	868.4	79.5	183.4	668.2	>1000	52.1												
C2209	52.6	26.7	40.7	12.5	48.2	214.0	107.3	341.9	214.9	58.8	44.0												
C2020	65.8	37.8	164.0	>1000	53.5	71.5	131.3	>1000	119.0	>1000	83.7												
C2221	69.3	26.4	47.6	>1000	58.8	>1000	355.2	>1000	46.3	>1000	124.0												
C2019	88.5	96.3	>1000	25.5	90.8	70.1	726.4	92.3	125.5	380.3	>1000												
C2110	118.4	106.6	92.6	>1000	109.9	797.4	254.9	198.0	301.5	>1000	218.3												
C2018	118.9	37.2	55.4	33.4	110.8	98.0	284.5	123.8	135.8	140.0	>1000												
C2022	153.4	61.6	114.5	>1000	130.5	>1000	247.7	358.7	162.8	>1000	139.2												
C2113	348.4	127.8	242.4	166.8	267.1	347.9	>1000	922.3	339.4	>1000	>1000												
C2149	376.8	178.6	259.3	>1000	331.2	>1000	724.8	>1000	>1000	>1000	608.0												
C2026	433.1	25.6	258.1	400.1	350.5	925.7	188.0	368.0	387.1	190.1	147.3												
C2150	591.0	57.5	672.9	496.9	413.7	783.8	240.8	406.4	543.2	202.1	199.1												
C2013	593.3	204.6	391.0	>1000	484.3	117.9	>1000	>1000	>1000	>1000	>1000												
C2185	670.6	116.1	440.0	239.1	494.6	818.2	412.8	759.7	485.4	246.7	251.1												
C2004	722.5	117.4	529.5	521.1	468.7	>1000	400.1	496.2	928.0	318.2	345.1												
C2140	840.9	124.4	706.9	839.5	778.2	>1000	648.7	866.7	815.5	481.7	497.8												
C2109	1000.0	198.7	572.6	825.0	336.9	>1000	960.0	762.2	620.2	691.7	464.7												

IC50 (ng/ml)

b

	wt		R683G		R346S		K417N		N440K		A475V		E484K		Q493R		N501Y		KEN		L452R		
C2039	1.9	0.5	1.0	0.7	1.2	1.0	>1000	1.4	2.3	>1000	>1000												
C2237	6.7	0.7	3.8	2.3	4.7	3.8	342.4	9.1	4.5	815.8	>1000												
C2049	10.0	5.2	7.1	319.9	9.6	65.5	10.9	17.5	12.8	>1000	7.2												
C2065	11.6	9.8	>1000	4.0	11.1	6.4	387.7	9.6	11.1	123.4	>1000												
C2319	13.3	6.3	8.7	>1000	10.2	131.2	7.7	28.4	297.3	>1000	8.5												
C2175	17.6	4.9	12.1	5.1	14.2	8.0	506.1	>1000	17.5	347.0	23.5												
C2219	20.7	9.8	13.0	5.2	19.4	35.1	>1000	369.6	13.7	>1000	>1000												
C2227	48.3	28.5	94.8	20.6	45.0	36.8	>1000	8.7	>1000	>1000	14.3												
C2047	49.1	40.4	145.2	>1000	48.8	53.2	168.6	>1000	96.8	>1000	123.4												
C2045	52.0	41.2	46.4	>1000	61.1	375.8	62.9	>1000	60.3	>1000	76.4												
C2188	90.8	45.7	64.3	>1000	56.6	743.4	134.8	>1000	>1000	>1000	119.6												
C2037	148.1	74.1	53.1	32.7	88.0	103.4	378.3	147.5	157.4	246.4	>1000												
C2228	178.4	145.9	124.1	70.2	132.2	>1000	770.5	>1000	197.9	886.3	785.3												
C2167	200.4	140.1	156.4	13.6	144.2	143.0	287.9	233.5	183.3	28.4	243.6												
C2318	351.9	126.5	262.1	113.7	241.7	335.9	286.4	311.0	477.8	244.8	231.4												
C2210	366.2	145.7	236.9	188.6	270.5	297.1	382.6	333.2	276.1	381.7	363.0												
C2317	429.2	549.9	>1000	105.5	296.6	282.1	>1000	305.6	387.5	>1000	>1000												
C2172	451.6	246.0	324.0	214.0	257.3	>1000	363.5	>1000	486.9	>1000	199.7												
C2070	584.0	532.7	856.2	260.7	529.0	709.6	884.3	629.7	802.5	838.8	578.2												
C2321	843.9	254.3	>1000	648.9	>1000	627.1	400.1	316.5	693.4	445.2	>1000												

IC50 (ng/ml)

a-b. IC₅₀ values for n=40 neutralizing antibodies isolated after prime (**a**) or 1.3 months post-boost (**b**) against indicated mutant SARS-CoV-2 pseudoviruses. Color gradient indicates IC₅₀ values ranging from 0 (white) to 1000 ng/ml (red).

Reporting Summary

Nature Portfolio wishes to improve the reproducibility of the work that we publish. This form provides structure for consistency and transparency in reporting. For further information on Nature Portfolio policies, see our [Editorial Policies](#) and the [Editorial Policy Checklist](#).

Statistics

For all statistical analyses, confirm that the following items are present in the figure legend, table legend, main text, or Methods section.

- | | |
|-----|-----------|
| n/a | Confirmed |
|-----|-----------|
- The exact sample size (n) for each experimental group/condition, given as a discrete number and unit of measurement
 - A statement on whether measurements were taken from distinct samples or whether the same sample was measured repeatedly
 - The statistical test(s) used AND whether they are one- or two-sided
Only common tests should be described solely by name; describe more complex techniques in the Methods section.
 - A description of all covariates tested
 - A description of any assumptions or corrections, such as tests of normality and adjustment for multiple comparisons
 - A full description of the statistical parameters including central tendency (e.g. means) or other basic estimates (e.g. regression coefficient) AND variation (e.g. standard deviation) or associated estimates of uncertainty (e.g. confidence intervals)
 - For null hypothesis testing, the test statistic (e.g. F , t , r) with confidence intervals, effect sizes, degrees of freedom and P value noted
Give P values as exact values whenever suitable.
 - For Bayesian analysis, information on the choice of priors and Markov chain Monte Carlo settings
 - For hierarchical and complex designs, identification of the appropriate level for tests and full reporting of outcomes
 - Estimates of effect sizes (e.g. Cohen's d , Pearson's r), indicating how they were calculated

Our web collection on [statistics for biologists](#) contains articles on many of the points above.

Software and code

Policy information about [availability of computer code](#)

Data collection IRIS by iMedRIS version 11.02 for clinical data collection and management; BD FACSDiva Software Version 8.0.2 for flow sorting; Glomax Navigator Promega V.3 for neutralization assays; Omega 5.11 by BMG Labtech was used for Elisa Assays.

Data analysis FlowJo 10.6.2 for FACS analysis; GraphPad Prism 9.1; Microsoft Excel 16.36; MacVector 17.5.4 for sequence analysis; Omega MARS V2.10 by BMG Labtech for luminometer; Glomax Navigator V.3 from Promega, Adobe Illustrator 2020, Igbblastn v.1.14 and Change-O toolkit v.0.4.540 were used to annotate antibody sequences. scripts and the data used to process antibody sequences are available on GitHub (https://github.com/stratust/igpipeline/tree/igpipeline2_timepoint_v2).

For manuscripts utilizing custom algorithms or software that are central to the research but not yet described in published literature, software must be made available to editors and reviewers. We strongly encourage code deposition in a community repository (e.g. GitHub). See the Nature Portfolio [guidelines for submitting code & software](#) for further information.

Data

Policy information about [availability of data](#)

All manuscripts must include a [data availability statement](#). This statement should provide the following information, where applicable:

- Accession codes, unique identifiers, or web links for publicly available datasets
- A description of any restrictions on data availability
- For clinical datasets or third party data, please ensure that the statement adheres to our [policy](#)

Data are provided in Supplementary Tables 1-8. The raw sequencing data and computer scripts associated with Figure 2 and Extended Data Fig. 3 have been deposited at Github (https://github.com/stratust/igpipeline/tree/igpipeline2_timepoint_v2). This study also uses data from "A Public Database of Memory and

Naive B-Cell Receptor Sequences" (<https://doi.org/10.5061/dryad.35ks2>), PDB (6VYB and 6NB6), cAb-Rep (<https://cab-rep.c2b2.columbia.edu/>), Sequence Read Archive (accession SRP010970), and from "High frequency of shared clonotypes in human B cell receptor repertoires" (<https://doi.org/10.1038/s41586-019-0934-8>).

Field-specific reporting

Please select the one below that is the best fit for your research. If you are not sure, read the appropriate sections before making your selection.

Life sciences Behavioural & social sciences Ecological, evolutionary & environmental sciences

For a reference copy of the document with all sections, see nature.com/documents/nr-reporting-summary-flat.pdf

Life sciences study design

All studies must disclose on these points even when the disclosure is negative.

Sample size	Sample size of 32 individuals was based on having no history of prior SARS-CoV-2 infection, and had received either Moderna (mRNA-1273) or Pfizer-BioNTech (BNT162b2) mRNA vaccination, and were able to come in for multiple blood donations after prime, and 1.3- or 5 months post-boost, between January 21 and July 20, 2021. Sample size was not predetermined by statistical method, but were chosen based on feasibility of enrolling participants into the study during the enrollment period. Enrollment of this sample size gave sufficient statistics for the effect sizes of interest.
Data exclusions	No data were excluded from the analysis.
Replication	All experiments successfully performed at least twice.
Randomization	This is not relevant, as this is an observational study.
Blinding	This is not relevant, as this is an observational study.

Reporting for specific materials, systems and methods

We require information from authors about some types of materials, experimental systems and methods used in many studies. Here, indicate whether each material, system or method listed is relevant to your study. If you are not sure if a list item applies to your research, read the appropriate section before selecting a response.

Materials & experimental systems

n/a	Involved in the study
<input type="checkbox"/>	<input checked="" type="checkbox"/> Antibodies
<input type="checkbox"/>	<input checked="" type="checkbox"/> Eukaryotic cell lines
<input checked="" type="checkbox"/>	<input type="checkbox"/> Palaeontology and archaeology
<input checked="" type="checkbox"/>	<input type="checkbox"/> Animals and other organisms
<input type="checkbox"/>	<input checked="" type="checkbox"/> Human research participants
<input checked="" type="checkbox"/>	<input type="checkbox"/> Clinical data
<input checked="" type="checkbox"/>	<input type="checkbox"/> Dual use research of concern

Methods

n/a	Involved in the study
<input checked="" type="checkbox"/>	<input type="checkbox"/> ChIP-seq
<input type="checkbox"/>	<input checked="" type="checkbox"/> Flow cytometry
<input checked="" type="checkbox"/>	<input type="checkbox"/> MRI-based neuroimaging

Antibodies

Antibodies used

1. Mouse anti-human CD20-PECy7 (BD Biosciences, 335793), clone L27
2. Mouse anti-human CD3-APC-eFluro 780 (Invitrogen, 47-0037-41), clone OKT3
3. Mouse anti-human CD8-APC-421eFluro 780 (Invitrogen, 47-0086-42), clone OKT8
4. Mouse anti-human CD16-APC-eFluro 780 (Invitrogen, 47-0168-41), clone eBioCB16
5. Mouse anti-human CD14-APC-eFluro 780 (Invitrogen, 47-0149-4), clone 61D3
6. Zombie NIR (BioLegend, 423105)
7. Mouse anti-human IgD-BV421 (Biolegend, 348226), clone IA6-2
8. Mouse anti-human CD27-FITC (BD Biosciences, 555440), clone M-T271
9. Mouse anti-human CD19-BV605 (Biolegend, 302244), clone HIB19
10. Mouse anti-human CD71-PerCPCy5.5 (Biolegend, 334114), clone CY1G4
11. Mouse anti-human IgG-PECF594 (BD Bioscience, 562538), clone G18-145
12. Mouse anti-human IgM-AF700 (Biolegend, 314538), clone MHM-88
13. Mouse anti-human IgA-VioGreen (Miltenyi Biotec, 130-113-481), clone IS11-8E10
14. Peroxidase Goat anti-Human IgG Jackson Immuno Research 109-036-088
15. Peroxidase Goat anti-Human IgM Jackson Immuno Research 109-035-129
16. Peroxidase Goat anti-Human IgA Sigma A0295

Validation

All antibodies are commercially available and validated by manufacturers. Additionally information can be found on product website, listed below.

1. <https://wwwbdbiosciences.com/en-us/products/reagents/flow-cytometry-reagents/clinical-discovery-research/single-color-antibodies-ruo-gmp/pe-cy-7-mouse-anti-human-cd20.335793>
2. <https://https://www.biolegend.com/en-us/products/zombie-nir-fixable-viability-kit-8657www.thermofisher.com/antibody/product/CD3-Antibody-clone-OKT3-Monoclonal/47-0037-42>
3. <https://www.thermofisher.com/antibody/product/CD8a-Antibody-clone-OKT8-OKT-8-Monoclonal/47-0086-42>
4. <https://www.thermofisher.com/antibody/product/CD16-Antibody-clone-eBioCB16-CB16-Monoclonal/47-0168-42>
5. <https://www.thermofisher.com/antibody/product/CD14-Antibody-clone-61D3-Monoclonal/47-0149-42>
6. <https://www.biolegend.com/en-us/products/zombie-nir-fixable-viability-kit-8657>
7. <https://www.biolegend.com/en-us/search-results/brilliant-violet-421-anti-human-igd-antibody-8215>
8. <https://wwwbdbiosciences.com/en-ca/products/reagents/flow-cytometry-reagents/research-reagents/single-color-antibodies-ruo/fitc-mouse-anti-human-cd27.555440>
9. <https://www.biolegend.com/en-us/products/brilliant-violet-605-anti-human-cd19-antibody-8483?GroupID=BLG5913>
10. <https://www.biolegend.com/en-us/products/percp-cyanine5-5-anti-human-cd71-antibody-9387?GroupID=BLG4836>
11. <https://wwwbdbiosciences.com/en-us/products/reagents/flow-cytometry-reagents/research-reagents/single-color-antibodies-ruo/pe-cf594-mouse-anti-human-igg.562538>
12. <https://www.biolegend.com/fr-lu/products/alexa-fluor-700-anti-human-igm-antibody-12507>
13. <https://www.miltenyibiotec.com/US-en/products/iga-antibody-anti-human-is11-8e10.html#gref>
14. <https://www.jacksonimmuno.com/catalog/products/109-036-088>
15. <https://www.jacksonimmuno.com/catalog/products/109-035-129>
16. <https://www.sigmaaldrich.com/US/en/product/sigma/a0295>

Eukaryotic cell lines

Policy information about [cell lines](#)

Cell line source(s)	293T (CRL-11268) and HT1080 (CCL-121) were originally obtained from ATCC. Based on these cell lines, we generated the following cells: 293T/ACE2* (Robbiani, D. et al. Nature 584, doi.org/10.1038/s41586-020-2456-9) HT1080/ACE2.cl14 (Schmidt, F. et al. J Exp Med 217, doi:10.1084/jem.20201181) Both the 293T/ACE2 and HT1080/ACE2.cl14 cell lines are obtained from the Laboratory of Retrovirology, Rockefeller University.
Authentication	Not authenticated after purchase from ATCC.
Mycoplasma contamination	The cells were checked for mycoplasma contamination by Hoechst staining, and confirmed negative.
Commonly misidentified lines (See ICLAC register)	No commonly misidentified cell lines were used.

Human research participants

Policy information about [studies involving human research participants](#)

Population characteristics	Participants were healthy volunteers receiving either the Moderna (mRNA-1273) or Pfizer-BioNTech (BNT162b2) mRNA vaccines against SARS-CoV-2 who were recruited for serial blood donations at Rockefeller University Hospital in New York between January 21 and July 20, 2021. Participants indicated as “Prime/1.3 post-Boost” were individuals who were de novo recruited for this study, while a subgroup of individuals (indicated as “1.3m/5m”) were from a long-term study cohort ¹² . Eligible participants were healthy adults with no history of infection with SARS-CoV-2, as determined by clinical history and confirmed through serology testing, receiving one of the two Moderna (mRNA-1273) or Pfizer-BioNTech (BNT162b2), according to current dosing and interval guidelines. Exclusion criteria included incomplete vaccination status, presence of clinical signs and symptoms suggestive of acute infection with or a positive RT-PCR results for SARS-CoV-2 in saliva, or a positive COVID-19 serology. Seronegativity for COVID-19 was established through the absence of serological activity toward the nucleocapsid protein (N) of SARS-CoV-2. Volunteers ranged in age from 23-78 years old (median = 34.5 years). 53% were male and 47% female.
Recruitment	Participants presented to the Rockefeller University Hospital for blood sample collection and were asked to provide details of their vaccination regimen, possible side effects, comorbidities and possible COVID-19 history. Recruitment was open to all eligible adults receiving an mRNA vaccine against SARS-CoV-2. Other than the criteria listed herein, no other parameters were used to exclude or include patients. Therefore, we cannot identify any factors that would lead to self-selection bias. All participants provided written informed consent before participation in the study and the study was conducted in accordance with Good Clinical Practice.
Ethics oversight	Institutional Review Board (IRB) at the Rockefeller University, protocol DRO-1006.

Note that full information on the approval of the study protocol must also be provided in the manuscript.

Plots

Confirm that:

- The axis labels state the marker and fluorochrome used (e.g. CD4-FITC).
- The axis scales are clearly visible. Include numbers along axes only for bottom left plot of group (a 'group' is an analysis of identical markers).
- All plots are contour plots with outliers or pseudocolor plots.
- A numerical value for number of cells or percentage (with statistics) is provided.

Methodology

Sample preparation	Whole blood samples were obtained from study participants recruited through Rockefeller University Hospital. Peripheral blood mononuclear cells (PBMCs) were separated by Ficoll gradient centrifugation. Prior to sorting, PBMCs were enriched for B cells using a Miltenyi Biotech pan B cell isolation kit (cat. no. 130-101-638) and LS columns (cat. no. 130-042-401).
Instrument	FACS Aria III (Becton Dickinson)
Software	BD FACSDiva Software Version 8.0.2 and FlowJo 10.6.2
Cell population abundance	Sorting efficiency ranged from 40% to 80%. This is calculated based on the number of IgG-specific antibody sequences that could be PCR-amplified successfully from single sorted cells from each donor.
Gating strategy	Cells were first gated for lymphocytes in FSC-A (x-axis) versus SSC-A (y-axis). We identify single cells in FSC-A versus FSC-H, and then SSC-A versus SSC-W. We then select for CD20+ Dump- B Cells in dump (anti-CD3-eFluro 780, anti-CD16-eFluro 780, anti-CD8-eFluro 780, anti-CD14-eFluro 780, Zombie NIR) versus CD20 (anti-CD20-PE-Cy7); dump-negative was considered to be signal less than 250, and CD20-positive was taken to be signal greater than 100. We then gate for Ova- B cells in FSC-A versus Ova-BV711; Ova-negative was considered to be all cells with signal less than 100. Select for Sars-CoV-2 RBD double-positive cells in RBD PE versus RBD AlexaFluor 647; this gate was made along the 45° diagonal, above 1000 on both axes.

- Tick this box to confirm that a figure exemplifying the gating strategy is provided in the Supplementary Information.